Contrib Mineral Petrol (2006) 151: 413–433
DOI 10.1007/s00410-006-0068-5

ORIGINAL PAPER

E. B. Watson · D. A. Wark · J. B. Thomas

Crystallization thermometers for zircon and rutile

Received: 29 August 2005 / Accepted: 18 January 2006 / Published online: 3 March 2006

Abstract Zircon and rutile are common accessory minerals whose essential structural constituents, Zr, Ti, and Si can replace one another to a limited extent. Here we present the combined results of high pressure–temperature experiments and analyses of natural zircons and rutile crystals that reveal systematic changes with temperature in the uptake of Ti in zircon and Zr in rutile. Detailed calibrations of the temperature dependencies are presented as two geothermometers—Ti content of zircon and Zr content of rutile—that may find wide application in crustal petrology. Synthetic zircons were crystallized in the presence of rutile at 1–2 GPa and 1,025–1,450°C from both silicate melts and hydrothermal solutions, and the resulting crystals were analyzed for Ti by electron microprobe (EMP). To augment and extend the experimental results, zircons hosted by five natural rocks of well-constrained but diverse origin (0.7–3 GPa; 580–1,070°C) were analyzed for Ti, in most cases by ion microprobe (IMP). The combined experimental and natural results define a log-linear dependence of equilibrium Ti content (expressed in ppm by weight) upon reciprocal temperature:

$$\log(\mathrm{Ti}_{\mathrm{zircon}}) = (6.01 \pm 0.03) - \frac{5080 \pm 30}{T\ (\mathrm{K})}.$$

In a strategy similar to that used for zircon, rutile crystals were grown in the presence of zircon and quartz (or hydrous silicic melt) at 1–1.4 GPa and 675–1,450°C and analyzed for Zr by EMP. The experimental results were complemented by EMP analyses of rutile grains from six natural rocks of diverse origin spanning 0.35–3 GPa and 470–1,070°C. The concentration of Zr (ppm by weight) in the synthetic and natural rutiles also varies in log-linear fashion with T^{-1}:

$$\log(\mathrm{Zr}_{\mathrm{rutile}}) = (7.36 \pm 0.10) - \frac{4470 \pm 120}{T\ (\mathrm{K})}.$$

The zircon and rutile calibrations are consistent with one another across both the synthetic and natural samples, and are relatively insensitive to changes in pressure, particularly in the case of Ti in zircon. Applied to natural zircons and rutiles of unknown provenance and/or growth conditions, the thermometers have the potential to return temperatures with an estimated uncertainty of ± 10 ° or better in the case of zircon and ± 20° or better in the case of rutile over most of the temperature range of interest (~400–1,000°C). Estimates of relative temperature or changes in temperature (e.g., from zoning profiles in a single mineral grain) made with these thermometers are subject to analytical uncertainty only, which can be better than ± 5° depending on Ti or Zr concentration (i.e., temperature), and also upon the analytical instrument (e.g., IMP or EMP) and operating conditions.

Communicated by T. L. Grove

E. B. Watson (✉) · D. A. Wark · J. B. Thomas
Department of Earth & Environmental Sciences, Rensselaer Polytechnic Institute, Troy, NY 12180, USA
E-mail: watsoe@rpi.edu

Introduction

Several properties of the accessory minerals zircon and rutile make them particularly suitable for a variety of geo- and thermochronological applications. These properties—manifested to varying degrees in the two minerals—include widespread occurrence (in terms of both rocks types and P–T stability), tendency to concentrate elements having radioactive isotopes, chemical and physical durability, and resistance to diffusive re-equilibration. Of the two minerals, zircon is particularly robust. It is also structurally accommodating to key isotopes (e.g., of U, Th and Lu), and has provided a wealth of information about the evolution of the continental crust over the past few decades. Recent developments in zircon geochronology and geochemistry are particularly exciting in their implications for the nature and thermal state of the

very early crust (Mojzsis et al. 2001; Wilde et al. 2001; Turner et al. 2004).

The same property of zircons that makes them so useful (i.e., their survivability) also means that they are commonly hosted by rocks other than those in which they originally crystallized. For this reason, establishing the origin of specific zircons can be difficult, and the possibilities are numerous: zircons crystallize in terrestrial environments ranging from the high pressure–temperature conditions of the upper mantle (e.g., Davis et al. 1976) to near-surface hydrothermal systems (e.g., Kerrich and King 1993). They have also been found in lunar rocks and in meteorites (e.g., Compston et al. 1984; Ireland and Wlotzska 1992).

A key piece of information that could shed light on the origin of out-of-context zircons is the temperature at which they crystallized. Knowledge of crystallization temperature would be invaluable as a constraint on provenance of zircons of all ages, and in establishing the conditions of formation of very ancient zircons in particular. The numerous impurities in zircon (e.g., Speer 1982; Belousova et al. 2002; Hoskin and Schaltegger 2003) suggest several possibilities for temperature-dependent uptake that could be calibrated for use as a thermometer. For reasons discussed below, we settled on Ti content as the most promising of these, and here we report the results of an investigation of Ti concentration in zircon coexisting with rutile (TiO_2) as a function of temperature over the range ~600–1,450°C. The study involved a combination of experimental approaches and analyses of natural zircons grown under well-characterized conditions. Titanium content of zircon depends strongly upon temperature, varying by more than three orders of magnitude over the ~850° temperature range investigated, and is relatively immune to changes in pressure. Our calibration thus constitutes a sensitive zircon crystallization thermometer that can be implemented for natural zircons using an electron microprobe (EMP) (if the crystallization temperature exceeds ~850°C) or an ion- or laser-ablation microprobe for zircons grown at lower temperatures. Although the thermometer has been rigorously calibrated for rutile-saturated conditions only, this apparent drawback is not serious for two reasons: first, because TiO_2 activity in crustal rocks is generally high; and, second, because Ti is also taken up in quartz, so our Ti-in-zircon calibration can be used in conjunction with that of Wark and Watson (2004) for Ti in quartz to eliminate the dependence upon rutile. In other words, partitioning of Ti between zircon and quartz also serves as an effective, if somewhat less temperature-sensitive, zircon crystallization thermometer.

Although the primary focus of this study was zircon, the fact that most of our experiments involved co-crystallization of zircon *and* rutile led to the possibility of developing an additional thermometer based on the Zr content of rutile. There exists ample motivation for the expanded effort: although neither as ubiquitous in the crust nor as survivable as zircon, rutile is nevertheless common, and occurs as a primary mineral in alkalic plutonic rocks and metamorphic rocks ranging from greenschist to eclogite facies. Rutile also concentrates U and other trace elements to a sufficient degree to make it suitable for age dating and constraining crustal thermal and metasomatic events (e.g., Mezger et al. 1989, 1991; Sorensen and Grossman 1989; Wong et al. 1991; Davis 1997; Zack et al. 2002). Moreover, Zack et al. (2004) have recently established that the Zr content of natural rutile shows systematic variations attributable to differences in crystallization temperature. From the standpoint of potential usefulness in thermometry, rutile actually has one advantage over zircon: rutile crystals usually grow in the presence of zircon (commonly accompanied by quartz), which means that in many cases the chemical potential of ZrO_2 in the system is essentially fixed. It is thus possible that most or all variations in Zr content of natural rutile crystals are attributable to differences in temperature (or possibly pressure; see Comparison with other studies and the effect of pressure).

Strategy and theoretical basis of the thermometers

Zircon

As noted above, zircons serve as host for a variety of trace elements. Among non-radioactive components, Hf is generally present in crustal zircons at the ~1–2% level, and total *Y* and the rare earth elements (REE) often exceed 1,000 ppm. Their high concentrations do not, however, make these elements promising for thermometry, because their chemical potentials (activities) are unknown. The Hf^{4+} ion, for example, enters the zircon lattice by direct exchange with Zr^{4+} (therefore requiring no coupled substitution or vacancy formation), but μ_{HfO_2} in geochemical systems is unconstrained, so uptake of Hf in zircon probably depends upon extensive variables as well as temperature. Yttrium and the REE are also highly compatible in the zircon lattice, but their activities are, again, poorly known and variable in the systems of interest. In addition, these elements exist as M^{3+} cations, so their incorporation into zircon may be influenced by the activities of other system components required for charge balance.

Titanium suffers from neither of the shortcomings just noted. As a tetravalent cation at relevant oxygen fugacities, Ti can engage in isovalent replacement of the structural cations of zircon with no charge-compensating substitution. Recent theoretical calculations indicate that the dominant substitution is $Ti^{4+} = Si^{4+}$ at all relevant temperatures (Harrison et al. 2005), which is consistent with the appreciable solubility of Ti in quartz (Wark and Watson 2004), where Si^{4+} is the sole cation. Perhaps the greatest advantage of Ti as a potential indicator of temperature is that its chemical potential in crustal systems is highly constrained, so observed variations in the Ti content of zircon and other silicate

minerals can be attributed more confidently to changes in intensive variables. Indeed, TiO_2 is nearly unique among minor elements of typical crustal rocks in being present at activities generally close to unity. Rutile is common in metamorphic rocks but much less so in igneous rocks; however, even in the absence of rutile itself, other Ti-based phases (titanite, ilmenite) and Ti-bearing silicates constrain TiO_2 activity to high values (in metapelites a_{TiO_2} is close to 1; in metabasalts it is generally ~0.6; Ghent and Stout 1984). The rutile saturation model of Ryerson and Watson (1987) and recent results of Hayden et al. (2005, 2006) also indicate high TiO_2 activities in siliceous silicate melts at geologically relevant temperatures (see Zircon). The one shortcoming of Ti content as an indicator of zircon crystallization temperature is that the concentration is quite low. The inherent incompatibility of Ti in zircon leads to expected levels in the 0.3–50 ppm range under most circumstances (corresponding to ~500–900°C).

The thermodynamic basis of the Ti-in-zircon thermometer is the simple reaction

$$TiO_{2(\text{rutile})} = TiO_{2(\text{zircon})}, \quad (1)$$

for which the equilibrium constant is

$$k_1 = \frac{a_{TiO_2}^{\text{zircon}}}{a_{TiO_2}^{\text{rutile}}},$$

where a_{TiO_2} is the activity of TiO_2 in rutile or zircon as indicated by the superscript. Because rutile is nearly pure TiO_2 (diluted slightly by Nb_2O_5 and other impurities), $a_{TiO_2}^{\text{rutile}} \sim 1$, so $k \cong a_{TiO_2}^{\text{zircon}}$. Therefore

$$a_{TiO_2}^{\text{zircon}} = \gamma_{TiO_2}^{\text{zircon}} X_{TiO_2}^{\text{zircon}} = \exp\left[\frac{-\Delta G_1^{\circ}}{RT}\right], \quad (2)$$

where γ is the activity coefficient and X the mole fraction of TiO_2 in zircon, ΔG_1° is the free energy change for reaction 1 when "reactant" and "product" are in their standard states, R is the gas constant, and T is absolute temperature. If $\gamma_{TiO_2}^{\text{zircon}}$ is assumed constant, then the logarithm of the Ti concentration in zircon is expected to be linear in T^{-1}.

Rutile

The reasoning summarized above for zircon applies almost in reverse to Zr in rutile, although it would not be conceptually accurate to think in terms of a zircon–rutile "solvus" because the minerals are not isostructural. At equilibrium, the relevant exchange reaction is

$$ZrO_{2(\text{zircon})} = ZrO_{2(\text{rutile})}, \quad (3)$$

which has an equilibrium constant

$$k_2 = \frac{a_{ZrO_2}^{\text{rutile}}}{a_{ZrO_2}^{\text{zircon}}}.$$

Thus, if $a_{ZrO_2}^{\text{zircon}} = c$ (a constant), then $k_2 \cong a_{ZrO_2}^{\text{rutile}}/c$ and

$$a_{ZrO_2}^{\text{rutile}} = \gamma_{ZrO_2}^{\text{rutile}} X_{ZrO_2}^{\text{rutile}} = c \ \exp\left[\frac{-\Delta G_2^{\circ}}{RT}\right]. \quad (4)$$

As with Ti in zircon, if $\gamma_{ZrO_2}^{\text{rutile}}$ is constant, then the logarithm of the Zr concentration in rutile should vary linearly with T^{-1}. Ignoring slight dilution by HfO_2, UO_2, ThO_2 and rare-earth oxides, $a_{ZrO_2}^{\text{zircon}}$ is constrained to a high and constant value if zircon coexists with quartz, which is frequently the case in natural systems. Zircon can coexist with baddeleyite in silica-undersaturated systems—in which case $a_{ZrO_2}^{\text{zircon}}$ would be buffered at a value close to unity; however, this situation is relatively uncommon in crustal rocks and not of primary interest in this study. The intermediate case (zircon coexisting with neither quartz nor baddeleyite) is also possible; here, $a_{ZrO_2}^{\text{zircon}}$ would be unbuffered but constrained between the limits of the previous two cases.

Experimental techniques

Overview

Zircon and rutile were co-crystallized in the lab over a wide range in temperature in order to explore and evaluate the dependencies 'predicted' by Eqs. 2 and 4. Most experiments were performed at ~1 GPa as a representative lower crustal pressure. Rutile crystals > 30 μm in size were readily grown at temperatures ranging from 675 to 1,450°C from both hydrothermal solutions and silicate melts using established solid-media (piston-cylinder) techniques. Zircons of analyzable size were more difficult to produce, and several different approaches were used (see below). These yielded 10- to 60-μm crystals falling into two broad categories: 'melt-grown' zircons crystallized from hydrous, siliceous melt, and 'hydrothermal' zircons grown from aqueous solution. At $T < 1{,}100°$, the hydrothermal zircons coexisted with rutile and quartz, but quartz was absent at higher temperatures because it is not stable at P_{H_2O} in excess of ~1 GPa (Kennedy et al. 1962). Two zircon-growth runs were made at 2 GPa in order to evaluate the possibility that pressure has a significant effect on Ti uptake in zircon.

Zircon details

Crystallization of hydrothermal and melt-grown zircons involved a variety of starting compositions and several different experimental configurations. Some were grown by reacting ZrO_2 with SiO_2 in the presence of fluid or melt, others from multicomponent glassy starting materials in which the ZrO_2 and SiO_2 were pre-dissolved at 1,500°C and atmospheric pressure. Still other experiments involved overgrowth, through coarsening, of new mantles on small zircon seeds dispersed in the starting materials. The small size of most of the synthetic zircons

necessitated analysis by EMP (see below), which was challenging because of the difficulties inherent in measuring low concentrations of Ti in small (often <20 μm) crystals in close proximity with Ti-rich phases (glass, rutile, quenched aqueous solute). In some cases, zircon seeds were maintained physically distant (by 1–2 mm) from rutile during the experiments by means of a nested capsule arrangement that relied upon aqueous diffusion to ensure equilibrium despite the separation of the phases. In other instances zircons and rutile crystals grown in close proximity from H_2O-saturated melt were removed from the quenched glass by dissolving the latter in concentrated HF. The zircons and rutiles were then dispersed in either epoxy or Pb-silicate glass (as an X-ray absorber) for polishing and EMP analysis. The various experimental configurations are shown schematically in Fig. 1. For experiments involving multi-component hydrous melts, the starting compositions are summarized in Table 1, which also provides additional details concerning bulk H_2O contents, pre-fusion steps, and added zircon. Starting solids for the hydrothermal experiments were coarsely ground quartz, commercial synthetic rutile and either synthetic zircon or stoichiometric ZrO_2 + SiO_2. Additional details of the hydrothermal experiments (added HF in the fluid; physical arrangement of materials) are indicated in Table 2. Although numerous efforts were made to grow zircons at temperatures below 1,000°C, the resulting crystals were too small for reliable analysis. Images of selected run products are shown in Fig. 2.

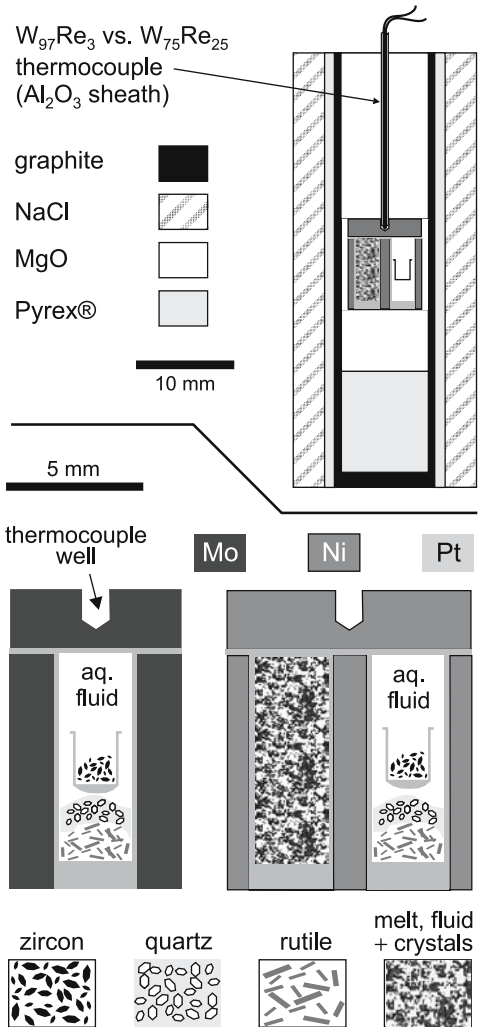

Fig. 1 Schematic representation of piston-cylinder assembly (*top*) and capsule arrangements (*bottom*) used in this study. The capsules are of a pressure-sealing design described in detail by Watson and Lupulescu (1993). When Ni is used as the "strong" metal ($T<1{,}200$°C), the metal is pre-oxidized to limit interdiffusion with Pt; in this case the internal oxygen fugacity is buffered at Ni–NiO. The arrangement with the (unsealed) internal Pt cup was used in hydrothermal experiments to isolate zircons from rutiles in the run products. See text for discussion

Natural samples

Because of the potential significance of the Ti-in-zircon thermometer for crustal igneous and metamorphic systems, it was considered essential to extend the calibration downward into the temperature range of general use, and to demonstrate consistency between experiment and nature. When it became clear that we could not obtain reliable experimental results for Ti in zircon at $T<1{,}000$°C, we undertook a search for natural zircons, preferably coexisting with rutile, whose growth circumstances could be established and whose crystallization temperatures could be estimated using independent geothermometers. The inherent survivability of zircon makes this task more difficult than it might seem. Emphasis was also placed upon samples for which effective diffusive communication between zircon and rutile could be reasonably assumed. We used magmatic zircons from a glassy volcanic rock and a well-characterized migmatite, as well as metasomatic (hydrothermal) zircons from deep crustal and upper mantle environments. Most samples were acquired as whole-rock hand specimens, from which zircon and rutile separates were obtained by conventional methods. The geologic histories of the zircons implied by their descriptions in the literature were confirmed, insofar as it was possible, by characterization of chemical zoning using cathodoluminescence (CL) and backscattered-electron imaging. Sample sources, descriptions and thermobarometry are summarized in the Appendix; selected CL images of zircons are shown in Fig. 3.

Zircons from five rocks—Adirondack migmatite (ADK), Bishop Tuff (BT), Stillup Tal aluminous schist (ST), Labait harzburgite (LB) and Santa Catalina migmatite (SC)—are used in combination with the high-temperature synthetic zircons as the basis for the Ti-in-zircon thermometer calibration. In these natural cases, the activity of Ti in the system is either directly known (for ADK, ST, LB and SC $a_{TiO_2}=1$ because rutile is present in the rocks) or calculable with few assumptions (BT; see Zircon). Moreover, the relevant temperatures of the natural systems are generally well constrained by

Table 1 Compositions of melts (weight % oxides) in experiments where zircon and rutile coexisted in H_2O-saturated silicate melts

Expt no. →	67	70	71	73	81	82b	91[c]	95[c]
SiO_2	70.0	60.0	60.0	84.5	70.0	80.5	58.0	58.0
TiO_2	7.9	10.2	10.2	6.2	6.4	4.0	4.0	4.0
Al_2O_3	6.8	6.9	6.9	–	–	3.4	18.0	18.0
FeO	0.4	0.4	0.4	–	–	0.2	–	–
MgO	0.1	0.1	0.1	–	–	–	5.0	5.0
CaO	0.3	0.3	0.3	–	–	0.1	5.0	5.0
Na_2O	1.9	2.0	2.0	–	–	1.0	4.0	4.0
K_2O	10.7	10.0	10.0	–	–	5.4	4.0	4.0
ZrO_2	11.0	10.1	10.1	–	–	5.5	2.0	2.0
Zircon[a]	–	–	–	9.3	23.6	–	–	–
H_2O[b]	19.4	18.4	19.1	5.4	20.3	6.9	24.5	19.3

[a]Synthetic, Hf-free zircon ground to <10 μm grain size
[b]$\frac{H_2O}{oxides + H_2O}$ (wt%) added to experimental container
[c]Oxides pre-fused at 1 atm (1,500°C)

independent geothermometers (see Appendix), and reasonable assumptions can be made about the timing of zircon growth. Zircons from five additional host rocks were analyzed, but the results—although generally consistent with the Ti thermometer—were not included in the actual calibration because of analytical and/or interpretational complexities (see section Zircon thermometry of selected rocks).

The Zr-in-rutile thermometer calibration is based mainly upon laboratory experiments at 1–1.4 GPa, spanning 675–1450°C. As with the Ti-in-zircon thermometer, however, analyses of rutile crystals in six natural rocks were used to extend the calibration to significantly lower temperatures—in this case ~470°C—with extensive overlap in temperature range with the experiments. Four natural rocks are common to the rutile and zircon thermometer calibrations: LB, ADK, SC and ST. The two additional samples included in the Zr-in-rutile calibration are a greenschist (GS) from central New England, USA (Spear et al. 2002) and a blueschist (SF) from Sifnos Island, Greece (Schliestedt 1986; Spear et al. 2006).

Table 2 Summary of run information and electron microprobe analyses of synthetic zircons. All zircons coexist with rutile

Run ID	Type[c]	*T* (C)	GPa	Time (h)	ppm Ti (2 s.e.)
52	HF	1,350	1.0	3.0	851 (36)
57	HDC(o)	1,400	1.0	3.0	1,353 (245)[a]
58	HDC(s)	1,200	1.0	12.0	250[b]
59	HDC(s)	1,100	1.0	92.0	242[b]
63	HDC(o)	1,250	1.2	24.7	343 (25)
65	HDC(o)	1,150	1.0	73.3	217 (32)
66	HDC(s)	1,050	1.0	144.1	108 (23)
67	HM	1,225	1.0	49.5	466 (19)
70	HM	1,280	1.0	42.8	676 (62)
71	HM	1,350	1.0	19.8	860 (44)
73	HM	1,450	1.0	12.0	1,213 (83)
81	HM	1,450	1.0	2.0	1,120 (196)
91	HM(hf)	1,025	2.0	86.8	112 (30)
95	HM	1,225	2.0	39.6	311 (32)

[a]The standard deviation is reported in this case because the run 57 crystals are clearly zoned. Based on Fig. 4, the rim concentrations (~1,000 ppm) are probably "correct", but the overall average value is shown here and plotted in the figure
[b]"Plateau" values from traverses of overgrowth rims on seed zircons (see text and Fig. 2c)
[c]Symbols designating experiment types:
HF: zircons grown from 1 M HF solution containing ZrO_2, SiO_2 and TiO_2
HDC: hydrothermal experiments performed using a double-capsule technique. (o) indicates crystallization of zircons from oxides; (s) indicates overgrowth on small seeds by coarsening (see text and Fig. 2c)
HM: zircons grown from H_2O-saturated melt (see Table 1 for compositions)
HM(hf): zircons grown from melt saturated with 1 M HF solution

Analysis details

Electron microprobe

The EMP was used for analysis of Ti in all zircons grown experimentally and some high-Ti natural specimens, and also for analysis of Zr in all rutiles, both synthetic and natural. The JEOL 733 at RPI was used in most cases, but our new Cameca SX 100 came on line toward the end of the study and was used in a few cases as noted later. The standards were Ti-free synthetic zircon (for Si and Zr) and synthetic rutile (for Ti). Analyses were performed with a focused beam at 15 kV accelerating potential and sample currents ranging from 50 to 200 nA; K_α X-rays were collected through PET and TAP crystals, respectively, for Ti and Si, and the L_α line was used for Zr (TAP crystal). Because the concentration of Ti in the synthetic zircons ranged down to values <100 ppm, acquisition times were sometimes as long as 300 s. During this counting interval, four of the five spectrometers on the JEOL and Cameca instruments were devoted to simultaneous counting of the Ti peak, and the four peak intensities were averaged at the end of the analysis to obtain a concentration. These procedures resulted in detection limits of ~12 and ~8 ppm Ti with the JEOL and Cameca instruments, respectively, which is suitable for zircons crystallized at or above ~900°C (where Ti ≈ 50 ppm). In most cases, however,

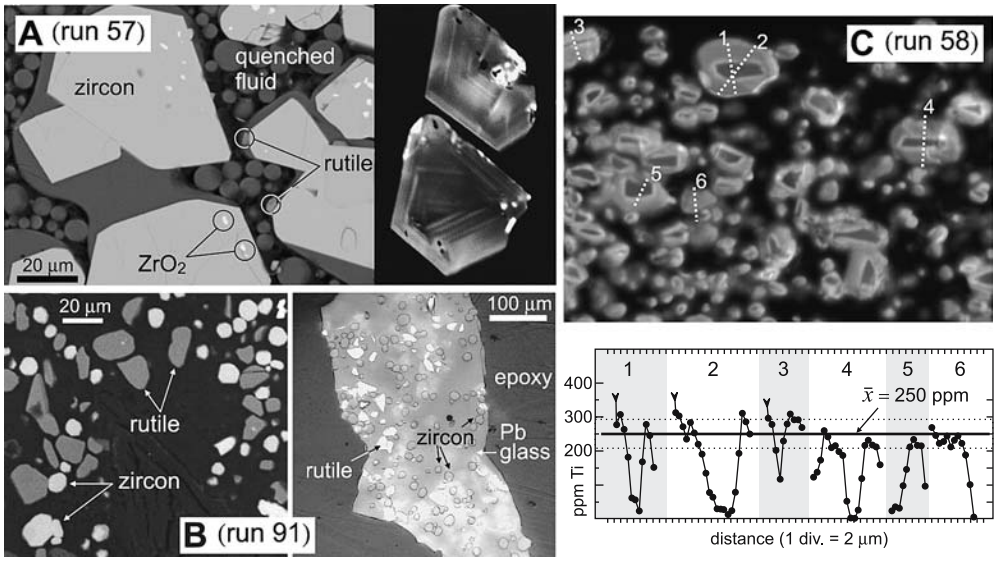

Fig. 2 Selected images of experimental run products. **a** Run 57 zircons, with quench material and typical ZrO_2 inclusions. *Left panel* is a backscattered-electron (*BSE*) image; *right panel* is a cathodoluminescence (*CL*) image. These are the largest, most Ti-rich zircons grown in this study, and have seen limited circulation for use as IMP standards (ANU, LLNL, UMD, WHOI, UWisc). **b** Zircons and rutiles from run 91. The *left panel* (BSE image) shows disaggregated grains mounted in epoxy; the *right panel* (reflected-light image) shows the same run products remounted in Pb-silicate glass as an X-ray absorber. This represents one of the lowest temperature runs from which meaningful data could be extracted. **c** *Top panel* is a CL image of zircons from run 58, produced by hydrothermal overgrowth of new mantles (*medium gray*) on small, Ti-free seed cores (*darker gray*). The *dotted white lines* identify EMP traverses; *numbers* correspond with plots in the *bottom panel*. The mean of all the apparent "plateau" values (250 ppm) is taken as the near-equilibrium Ti content of zircons grown at run conditions. The *arrowheads* on scans 1–3 indicate high Ti values due to X-ray contributions from Ti-rich quench material deposited on top of the zircons during quench (similar to the more voluminous quench material in **a**). See text, Fig. 1 and Table 2 for details and discussion

detectability of Ti was not the limiting factor in the synthetic zircon analyses. The small size of the crystals and the coexistence with rutile and other Ti-rich phases during the experiments led to severe problems with secondary fluorescence of Ti during the analyses. The suspected occurrence of this phenomenon was confirmed by performing analytical traverses across the zircon/rutile interface of a blank couple of the two minerals fabricated for the purpose. Once the extent of the problem was understood, measures were taken to minimize the effect. As described briefly in Experimental techniques, run products were treated in HF to dissolve Ti-bearing glass or vapor-phase quench material adhering to the zircons. Rutile crystals did not dissolve in the acid treatments, but in many cases the residual zircon and rutile could be effectively dispersed during preparation of a mount for EMP analysis (see Fig. 2).

As noted above, the EMP analysis of both synthetic and natural rutile crystals for Zr was straightforward because the crystals generally exceed 50 μm in minimum dimension, and because the concentrations are relatively high (even at 675°C, the equilibrium Zr content of rutile coexisting with zircon is ~430 ppm). Analytical procedures varied depending on the specific samples being analyzed, but by dedicating four spectrometers to Zr and using long counting times, a minimum detection limit (MDL) of ~25 ppm was achievable with the JEOL 733 and ~18 ppm with the Cameca SX 100.

Ion microprobe (IMP): general operating conditions

Given the ~10 ppm MDL for EMP analysis of Ti in zircon (see above), an alternative instrument was needed for accurate and precise analysis of natural zircons grown at temperatures well below the 1,025–1,450°C experimental range. For this purpose we used the Cameca ims 3f IMP at Woods Hole Oceanographic Institution (WHOI; The Northeast National Ion Microprobe Facility). Implementation was relatively straightforward because the experimental phase of the study produced suitable standards: some of the high-temperature experiments yielded relatively large zircons whose Ti contents could be accurately determined by EMP. Run 57 zircons range up to 100 + μm in size and contain ~1,350 ppm Ti; run 59 zircons range up to 40 μm and contain ~240 ppm. In combination with nominally Ti-free synthetic zircon (see Watson et al. 1997), these crystals constitute a suitable set of standards easily covering the natural range in Ti concentration. The run 57 zircons do exhibit core-to-rim zoning in Ti (~2,000–1,000 ppm in the most extreme case), and some also contain small inclusions of relatively Ti-rich ZrO_2. However, the latter are easily avoided by reference to backscattered electron images and monitoring ^{30}Si counts during the Ti analyses. The zoning in any given crystal was characterized by EMP prior to the IMP analyses. On seven separate visits to the WHOI ion probe facility, we developed a standard working curve

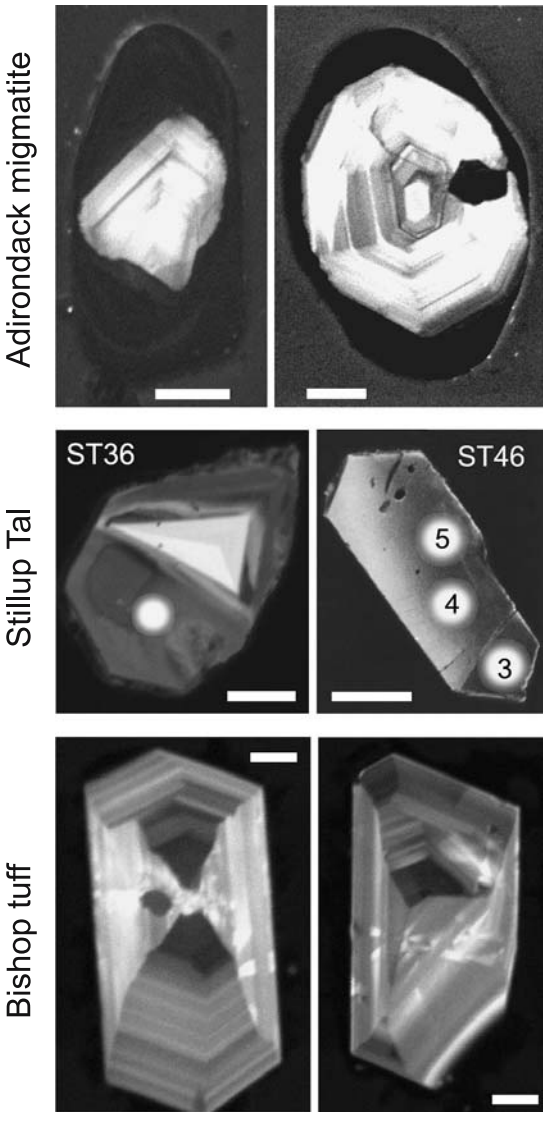

Fig. 3 Selected cathodoluminescence (CL) images of zircons from three rocks included in this study. *Top frame* Images of sectioned Adirondack migmatite (ADK) zircons showing typical CL-dark mantles; reported IMP analyses were confined to these mantles. *Middle frame* CL images of two of the five Stillup Tal (ST) zircons that yielded the lowest Ti concentrations. The large, CL-dark tip (lower half) of the sectioned zircon on the left contains 1 ppm Ti. The *right image* is of an unsectioned zircon—a polished facet—that is uniformly low in Ti (~1.4 ppm). *White circles* show locations of IMP analysis spots (numbers correlate with analyses in Table 3). *Bottom frame* Sectioned Bishop tuff (BT) zircons showing lack of inherited cores and continuous core → rim growth zoning superimposed on sectoral zoning. The *white scale bars* represent ~30 μm in all images

for run 57 zircons by cross-correlating specific analysis spots between the EMP and the IMP. The run 59 zircons (242 ppm Ti; homogeneous within our measurement ability) were used as a secondary IMP standard.

For most IMP analyses, a primary (O^-) ion beam current of 5 nA was used, which resulted in a spot size of 15–20 μm. With four 30-s acquisition intervals at each spot, we obtained a MDL of ~0.1 ppm Ti. Although adequate for our purposes, this MDL was higher than anticipated because we were forced to use the relatively low-abundance isotope ^{49}Ti (5.5% of Ti) for analysis of zircons specifically. Titanium-48 (74% abundance) would be preferable, but interference of $^{96}Zr^{2+}$ (2.8% isotopic abundance) with $^{48}Ti^+$ is unavoidable [Note that this interference also occurs in the analysis of zircons for Ti by LA-ICP-MS (CH Langmuir, personal communication 2005)]. The MDL for Ti analysis of quartz (Wark and Watson 2004) with the Cameca ims 3f is roughly an order of magnitude lower than for zircon because the ^{96}Zr interference with ^{48}Ti is absent. For zircons, the analytical uncertainty in Ti content using the Cameca 3f is $\sim \pm 6$ and $\pm 20\%$ at the 10 and 1 ppm levels, respectively. See Concluding remarks: application considerations for additional cautionary remarks pertaining to low-level Ti analysis in zircons by IMP (and LA-ICP-MS).

Analysis of natural zircons and rutiles: strategies and complications

The 15–20 μm primary ion beam made it possible to perform multiple analyses on individual natural zircons with the Cameca ims 3f, including what appeared in CL images to be distinct cores and rims of some crystals. In many cases, however, the spot was too large to resolve fine-scale zoning that might be present, or to obtain unequivocally "clean" analyses of the features of interest. Some explanation of the strategy and choice of analysis spots is thus required.

Zircons from the ADK have CL-dark overgrowth rims ranging up to ~30 μm in thickness (Fig. 3). These rims are interpreted as having grown near peak T conditions somewhat above the solidus (Storm and Spear 2005; see Appendix). However, it is likely that some rim growth occurred during subsequent crystallization of the melt and cooling of the migmatite body, so the rims may record a range in temperature. However, if new zircon growth was largely restricted to a period of eutectic-like (i.e., relatively isothermal) solidification of the melt, then this range was probably quite limited. In any case, the rims of ADK zircons were easy to distinguish in CL and sometimes relatively thick, so we could obtain "pure" rim analyses fairly easily. This was done on cross-sections through the zircons (as in Fig. 3) and also by polishing "flats" on the outer surfaces of some crystals to barely expose rim material. In both cases, we confirmed by post-analysis microscopy that the probe pits were fully confined to the CL-dark rim material. These precautions notwithstanding, the ion-probe spot size was too large to characterize intra-rim zoning of Ti, so for the ADK zircons we report all ion-probe analyses that could be confirmed by CL as representing rim material (10 analyses, ranging from 7.3 to 13.6 ppm). In the ADK case, it seems probable that the highest values represent the peak temperature of the anatectic event and the

lowest values the solidus (790 and 740°C, respectively; Storm and Spear 2005).

The ST zircons were more problematic because the distinction between ubiquitous relict (inherited) cores and new metamorphic growth was not as obvious as in the ADK case (see Fig. 3), and apparent rims and new crystal tips rarely exceeded a few microns in minimum dimension. Material inferred to have grown at peak metamorphic conditions is usually dark in CL, but dark zones are also present in the relict cores. Numerous cores were analyzed in order to confirm that these have Ti concentrations distinct from the rims. The cores contain 12–13 ppm Ti, indicating minimum growth temperatures of ~760°C, which is consistent with the granodioritic "protolith" of the aluminous schist from which the zircons were recovered (Selverstone et al. 1991; see Appendix). In general, the ion-probe beam was too broad to obtain "clean" analyses of the zircon rims in cross section. We looked for distinctive, CL-dark tips, corners or filled embayments on sectioned zircons, and we also analyzed surfaces exposed by gentle polishing or acid cleaning of crystal facets. For the ST case, we report the *lowest* measured Ti concentrations (8 analyses; 5 separate crystals), in the belief that these represent the least "contaminated" analyses of zircon grown during the metamorphic event recorded by the major-phase thermometers used for the aluminous schist (Selverstone et al. 1991). The locations of 4 of the 8 low-Ti analysis spots (1.0–1.6 ppm) are superimposed on CL images of the zircons in Fig. 3.

In the case of zircons from the BT, systematic core-to-rim diminution in Ti content may exist as a consequence of igneous zircon growth in a cooling regime. As in the ST case, such zoning would not necessarily be resolvable with a ~20-μm beam, especially in the smaller zircons. In the BT zircons, we were interested mainly in the Ti content of the zircon acquired during the pre-eruption interval of the BT magma, because this is the temperature recorded by the independent petrologic indicators. We attempted, nevertheless, to obtain compositions of the outermost rims by analyzing what amounted to polished growth facets, as in the case of the ST zircons. In contrast to the ST case, however, this "surface analysis" approach to the IMP measurements yielded values for the BT zircons similar to both near-rim and apparent core measurements made on zircons sectioned roughly through the middle of the crystal. We report all Ti analyses obtained on BT zircons ($n = 9$; 3.6–5.4 ppm); there is no statistically significant core–rim spatial correlation.

Zircons in the SC (garnet amphibolite) migmatite are optically clear and euhedral, and range between ~50 and ~200 μm in size. Imaged in CL, they generally lack distinct or sharp zoning, although some have cores that are noticeably brighter or darker than the rims. Multiple analyses were possible on a few of the largest grains, but no significant intragrain differences were discernible. The vast majority of the Ti contents of SC zircons fell in the 3–6 ppm range, but there were also two (apparent) values in excess of 25 ppm. These were discarded as outliers, probably representing relict cores.

The LB zircons (sample no. LB-17 of Rudnick et al. 1999) occur in diffuse veins with other metasomatic minerals (including rutile), and range up to ~600 μm in maximum dimension [the zircons analyzed in this study are the same ones that appear in Fig. 2 of Rudnick et al. (1999)]. Because these zircons crystallized at relatively high temperature (~1,070°C; see Appendix) they contain enough Ti (~100 ppm) to measure accurately by EMP. A total of 120 analyses (including two rim-to-rim traverses) were performed on three individual zircons, mostly using the Cameca SX 100.

As noted previously, Zr concentrations in the natural rutile crystals were sufficiently high to measure by EMP in all cases. The generally large grain size and good spatial resolution of the electron beam enabled thorough evaluation of both intra- and inter-grain variability (both are apparent in most of the rocks included in the study; see below).

Results and discussion

Zircon

The Ti concentrations of experimental and natural zircons are summarized in Tables 2 and 3, respectively, and are plotted against crystallization temperature in Fig. 4. For the synthetic zircons, the results are presented as straightforward averages of EMP analyses. The complexities encountered in some of the IMP analyses were discussed in the previous section, where it was made clear that only selected (low-Ti) data were used for the ST zircons. Titanium measurements on the BT zircons require special consideration for a different reason: the host rock was saturated in ilmenite rather than rutile (implying sub-unity TiO_2 activity), so the Ti contents of these zircons must reflect the reduced chemical potential of TiO_2 in the magma. Fortunately, the measured Ti contents can be adjusted for comparison with the rutile-saturated case *if an independent estimate of* a_{TiO_2} *in the magmas can be obtained*. This has recently become possible using two separate approaches. First, in quartz-saturated melts the TiO_2 content of quartz in equilibrium with rutile is now known (the 'TitaniQ' thermometer; Wark and Watson 2004). Somewhat surprisingly, Ti is more compatible in quartz than in zircon, and the concentration in "rutile-saturated" quartz can be measured by EMP down to temperatures as low as 650°C, where Ti is present at the ~30 ppm level. The BT contains abundant quartz phenocrysts, and we measured Ti concentrations in these crystals by both EMP and IMP. The BT phenocrysts have Ti distributions indicative of an abrupt increase in temperature at a late stage of growth (see Wark et al. 2004). In eruption package IG2Ea (stratigraphic nomenclature of Wilson and Hildreth 1997)—the source of the pumice from which the analyzed zircons were separated—most

Table 3 Titanium analyses of natural zircons used in this study. All are ion microprobe values except in the case of the Labait harzburgite zircons, which were analyzed by electron microprobe (see text)

Zircon/spot ID	$^{49}Ti/^{30}Si$	ppm Ti
Adirondack migmatite		
A4	0.000200	12.1
A8	0.000177	10.7
A8b	0.000161	9.8
A9	0.000143	8.7
A16	0.000149	9.0
A25	0.000153	9.3
A27	0.000224	13.6
A28	0.000148	9.0
A31	0.000120	7.3
A33	0.000178	10.8
Stillup Tal aluminous schist		
ST36	0.000016	1.0
ST46-3	0.000019	1.2
ST46-4	0.000021	1.3
ST46-5	0.000023	1.4
ST49-1	0.000024	1.5
ST49-2	0.000025	1.5
ST205h	0.000027	1.6
ST205m	0.000027	1.6
Bishop Tuff		
BT1core	0.000095	5.2 → 8.6[a]
BT1core	0.000096	5.2 → 8.7[a]
BT1rim	0.000082	4.5 → 7.5[a]
BT7rim	0.000069	3.8 → 6.3[a]
BT7core	0.000070	3.8 → 6.4[a]
BT11rim	0.000066	3.6 → 6.0[a]
BT12rim	0.000080	4.4 → 7.3[a]
BT13rim	0.000099	5.4 → 9.0[a]
BT15rim	0.000091	5.0 → 8.3[a]
Santa Catalina migmatite		
MM1b-1	0.000065	3.9
MM1b-3s	0.000097	5.9
MM1b-5	0.000052	3.2
MM1b-6a	0.000057	3.5
MM1b-7	0.000049	3.0
MM1b-10	0.000056	3.4
MM1b-10a	0.000054	3.3
MM1b-11	0.000090	5.5
MM1b-12c	0.000053	3.2
MM1b-12b	0.000086	5.2
Labait harzburgite		
JEOL 733		
14 Spots on 6 zircons		103 ± 9
Cameca SX 100		
60-Spot traverse, xtl no. 1		113 ± 8[b]
46-Spot traverse, xtl no. 2		107 ± 9[b]

[a] Arrow indicates upward adjustment made to correct for undersaturation in rutile (see text)

[b] The traverses reveal that both these crystals have compositionally uniform regions containing ~90 ppm Ti over much of the sectioned surface. Higher concentrations occur in localized patches, generally near the margins. The 90 ppm value is used in Fig. 4 because it is typical of most of the sectioned surfaces

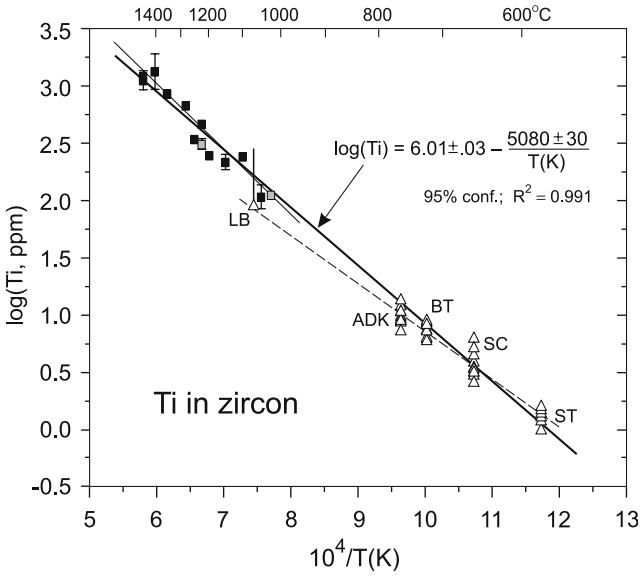

Fig. 4 Ti analyses of synthetic (*squares*) and natural (*triangles*) zircons plotted against $1/T$ (*black* 1 GPa; *gray* 2 GPa). The *heavy solid line* is the "global" fit to all data. The *light solid* and *dashed lines* are independent fits to the experimental and natural data, respectively. See text and Appendix for explanation and discussion

of the quartz phenocryst core growth is thought to have occurred at ~720–730°C and the thin, late-formed rim at temperatures as high as ~780°C. No appreciable zircon growth would be expected during the late, high-T phase (indeed, slight dissolution may have occurred, which would be consistent with our observation that core and rim Ti contents of the zircons are essentially the same). Accordingly, we assume the zircons grew at 725°C—i.e., corresponding to the main growth interval for quartz. The cores of the BT quartz phenocrysts average ~45 ppm Ti. If this quartz were in equilibrium with rutile (i.e., $a_{TiO_2} = 1$) at the growth temperature of 725°, it would contain ~75 ppm Ti. Assuming Henrian behavior of Ti in quartz, we can divide the measured Ti concentration by that expected for rutile saturation to obtain a_{TiO_2} in the system: 45/75 ppm = 0.6. This reduced a_{TiO_2} value allows us to adjust measured Ti concentrations in zircon to reflect the undersaturation of the system in rutile. This adjustment is shown in Table 3, and the adjusted concentrations of Ti in BT zircons are plotted in Fig. 4.

The high apparent TiO_2 activity in the BT may seem surprising given the fact that the mean Ti content of BT glass and melt inclusions in quartz is only 430 ppm (Peppard et al. 2001; Dunbar and Hervig 1992). Note, however, that many silicic magmas are saturated in a titaniferous phase of some kind (ilmenite, Ti-magnetite, titanite), and that once saturation in such a phase is achieved, it will generally be maintained (crystallization even of rutile, for example, cannot pull down the concentration of TiO_2 in the melt below the saturation value, so the system remains rutile-saturated, with $a_{TiO_2} = 1$, as igneous fractionation proceeds).

The second, complementary approach to evaluating TiO_2 activity in the BT melt is to assess proximity to saturation of the melt in rutile. Previous studies of rutile saturation in magmas indicate low values for silicic systems at low temperature. With significant

extrapolation beyond the range of experimental calibration, the rutile solubility model of Ryerson and Watson (1987) predicts a saturation value of ~1,500 ppm TiO_2 for the BT magma at pre-eruption temperature. The Ryerson–Watson (R–W) approach was recently extended by Hayden et al. (2005) to highly siliceous compositions (trondhjemite, s-type granite, metaluminous granite) at temperatures approaching those of direct geologic relevance. Although broadly consistent with the R–W calibration, the new results indicate substantially lower rutile solubilities equivalent to ~600–700 ppm Ti in the BT melt at relevant conditions. Again assuming Henrian behavior of TiO_2 in the melt, this result provides an independent estimate of a_{TiO_2} (implicitly referenced to pure liquid TiO_2) by dividing the measured Ti content of the BT magma by the measured rutile solubility. Hayden et al. (2005) also demonstrated that rutile solubility (and, by inference, TiO_2 activity) in siliceous melts is independent of H_2O content over the 6–12 wt% range. The relation given by Hayden et al. (2005) in their published abstract is based on their new data for rutile solubility in siliceous melts *combined with* the 'old' data of Ryerson and Watson (1987)—i.e., a general model for a broad range of magma types. More useful in the present context is a relation describing rutile solubility in siliceous melts that are likely to be saturated in zircon, which Hayden et al. (2006) express as

$$\log\left(\mathrm{Ti}_{\mathrm{sat}}^{\mathrm{melt}}\right) = \left[7.553(\pm 0.105) - \frac{4811(\pm 111)}{T(\mathrm{K})} + 0.114(\pm 0.023)\mathrm{FM}\right], \quad (5)$$

where $\mathrm{Ti}_{\mathrm{sat}}^{\mathrm{melt}}$ is the level of Ti (ppmw) in the melt required for saturation in rutile and FM is the same melt composition parameter used by Ryerson and Watson (1987); that is, FM = {[Na + K + 2(Ca + Fe + Mg)]/Al}/Si, where the chemical symbols represent cation fractions in the melt. Equation 5 applies to 1 GPa pressure, but Ryerson and Watson (1987) demonstrated that the pressure effect is small over the range of conditions relevant to the crust.

The need to adjust the TiO_2 concentrations of the BT zircons to make them consistent with rutile saturation may slightly weaken their contribution to the overall Ti versus T calibration, but this is offset by their great value in establishing general consistency between igneous zircons with relatively simple histories (i.e., the BT zircons) and metamorphic/hydrothermal zircons with complex histories (the ST, SC and ADK zircons).

A different (minor) complication arises in the interpretation of Ti analyses of the LB zircons (obtained by EMP). The three grains analyzed are homogeneous over most of their sectioned areas, but they exhibit Ti-rich patches (up to ~800 ppm Ti) of uncertain origin. Unlike the thin, Zr-rich rims on Labait rutiles, these Ti-rich regions do not form distinct outer zones around the entire grain perimeter; rather, they are localized areas occurring generally but not exclusively at the margins of the grains. The Zr-rich rims of the LB rutile grains are logically attributed to the pre-eruption heating event experienced by the harzburgite (see Appendix and Rudnick et al. 1999). For lack of an alternative explanation, we conclude that the Ti-rich patches of the zircons formed during the same event, and that the response to abrupt heating of zircon was simply different from that of rutile (which seems to have experienced simple "in-diffusion" of Zr; see Appendix). In both the zircon and rutile cases, we use the uniform "background" levels of Ti and Zr, respectively, for the purpose of the thermometer calibrations (Fig. 10). The compositional range of the high-Ti patches of the Labait zircons is indicated by the dotted line extending above the plotted symbol in Fig. 4.

A linear regression of all data in Fig. 4 yields the following relationship between Ti concentration in zircon (in ppm by weight) and temperature:

$$\log(\mathrm{Ti}) = (6.01 \pm 0.03) - \frac{5080 \pm 30}{T\ (\mathrm{K})}, \quad (6)$$

which has the form expected on the basis of simple thermodynamic reasoning (see Strategy and theoretical basis of the thermometers). The quoted uncertainties are at the 2σ level, determined using the least-squares fitting routine in Origin® (v. 7, Microcal Corp.). Uncertainty in Ti content only (i.e., in the dependent variable) was used in the fitting. This choice was made because the uncertainty in temperature of the experiments is very small, and the uncertainties in the crystallization temperatures of the natural zircons are difficult to assess. The observed range in Ti values of the natural zircons are well outside the IMP analytical uncertainty, and may reflect real variation in crystallization temperature. Lacking the ability to correlate Ti content with radial position in a zircon crystal or overgrowth rim (and hence with relative temperature), we plotted all the data for a given rock at the temperature estimated by previous workers using major-phase thermometers and phase equilibria (see Appendix). This approach involves the fewest arbitrary assumptions, even if it might not lead to the smallest estimated uncertainty in Eq. 5. A least squares fit to the experimental data alone (with Ti analytical uncertainties) yields a slope of −5,700 (±460) and an intercept of 6.44 (±0.23) for a line analogous to Eq. 6. The large uncertainty and consequent risk in down-temperature extrapolation (see Fig. 4) underscores the importance of the natural zircon Ti data to this study. A separate fit to the natural data is also shown in Fig. 4 (slope = −4,180 ± 150; intercept = 5.05 ± 0.16). This relation yields temperatures that deviate from those returned by the "global" fit (Eq. 6) by roughly +15° at ~560°C and −50° at 900°C, crossing over at ~650°C. Given the similarity of the "global" and "natural" fits over the region of prime interest in zircon

thermometry—especially for Hadean samples (Watson and Harrison 2005)—some users of the zircon thermometer may prefer to disregard the experimental results. Our view is that the experimental and natural data sets have differing strengths and weaknesses, so it makes sense to treat them as complementary and mutually reinforcing. The synthetic zircons are not immune to analytical difficulties, but the crystallization temperatures are very well constrained.

An important aspect of Eq. 6 is that it incorporates data pertaining to a significant range in pressure: the experiments were conducted at ~1 and 2 GPa (see Table 2), and the natural zircons crystallized at upper crustal pressures in the case of the BT (Wallace et al. 1999) and ~0.7–1.1 GPa for the ADK, SC and ST samples (Storm and Spear 2005; Sorensen and Barton 1987; Selverstone et al. 1991). Within uncertainty, all data fall on the same line, which indicates that the effect of pressure on Ti uptake is relatively small over the range relevant to the Earth's crust (but see Comparison with other studies and the effect of pressure).

Rearranged for direct use in thermometry, Eq. 6 becomes

$$T(^{\circ}\mathrm{C})_{\mathrm{zircon}} = \frac{5080 \pm 30}{(6.01 \pm 0.03) - \log(\mathrm{Ti})} - 273. \qquad (7)$$

The uncertainties in the constants lead to an uncertainty envelope on a T(°C) versus Ti plot, which is most easily appreciated from a plot of (2σ) uncertainty in temperature (ΔT) as a function of temperature (Fig. 5). This figure portrays the uncertainty in the absolute temperature returned by Eq. 7 for a specific Ti concentration. Additional uncertainty due to analytical error in the determination of Ti content will contribute to the overall uncertainty of a temperature estimate from a single analysis. At the operating conditions used with the Cameca ims 3f, analytical uncertainty adds $\sim\pm 1°$ (2σ) at 740° and $\sim\pm 6°$ at 570°C to the inherent uncertainty in a given temperature determination. In the bottom panel of Fig. 5 is a curve indicating the uncertainty in temperature arising solely from analytical error for the ion-probe conditions we used (clearly, this curve will be instrument-dependent). A curve is also included for EMP analysis of Ti in zircons at temperatures exceeding ~850°C.

In closing this section, it is important to emphasize that relative *differences* in apparent temperature (as opposed to the estimated absolute temperature) are subject to the analytical uncertainty only, because the error in the thermometer is the same for all determinations. For this reason, quite small differences in Ti concentration among analysis points within a single crystal (for example) will generally reflect real differences in temperature, even if the actual temperature is subject to significant uncertainty. Watson and Harrison (2005) took advantage of this fact to show a core-to-rim drop in crystallization temperature across a single Hadean zircon.

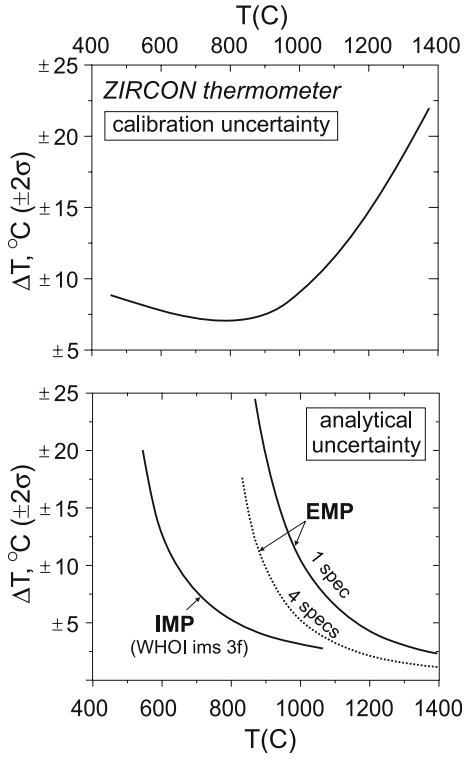

Fig. 5 Representation of the uncertainties in temperature estimates obtained with the Ti-in-zircon thermometer. *Top* 2-σ uncertainty inherent in the calibration itself, based on the least-squares fit to the combined experimental and natural data (Fig. 4; Eq. 6). *Bottom* Uncertainties resulting from counting statistics for X-rays (*EMP*) and ions (*IMP*). Note that these analytical errors are only approximately symmetric about the "target" temperature value, especially at values exceeding $\sim\pm 15°$. The EMP errors shown are for the RPI Cameca SX 100 operating at a 200-nA sample current and counting for 200 s (other operating conditions are described in the text). *Curves* are shown for X-ray counting with a single spectrometer and four spectrometers simultaneously. The calibration uncertainty applies to knowledge of absolute temperature; the analytical uncertainty alone affects knowledge of relative temperature

Rutile

Results of this study

Zirconium contents of experimental and natural rutile crystals are summarized in Tables 4 and 5, respectively, and are plotted against estimated crystallization temperature in Fig. 6. Table 4 contains information on the number of crystals analyzed in each rock and the analytical protocols used. The variation in Zr contents of rutile crystals in most rocks is well outside of the analytical uncertainty, with intergrain variations generally larger than those occurring within individual grains. The ADK rutiles, in particular, exhibit large grain-to-grain variations, with differences in Zr concentration approaching a factor of 4. This may be a consequence of partial diffusive re-equilibration of some grains (see Diffusion issues: preview of new data for Zr in rutile and speculations on Ti in zircon),

Table 4 Summary of run information and electron microprobe analyses of synthetic rutile crystals coexisting with zircon and quartz (below ~1,100°C) or siliceous, hydrous melt

Run ID	Type[a]	*T* (C)	GPa	Time (h)	ppm Zr (2 s.e.)
36	TZS	1,100	1.0	72.0	12,565 (792)
53b	HF	1,450	1.0	1.0	89,525 (2,849)
56a	HM	925	1.0	68.8	5,457 (2,673)
56b	HDC	925	1.0	68.8	3,084 (635)
58	HDC	1,200	1.0	12.0	20,330 (1,380)
62a	HDC	1,000	1.4	138.5	5,406 (341)
63	HDC	1,250	1.3	24.7	21,890 (3,924)
65	HDC	1,150	1.0	73.3	13,544 (1,001)
68a	HDC	950	1.0	240.0	4,670 (283)
69a	HDC	875	1.0	454.2	2,772 (198)
71	HM	1,350	1.0	18.9	63,100 (1,542)
73	HM	1,450	1.0	12.0	61,600 (2,137)
82b	HM	1,100	1.0	63.4	7,076 (498)
87a	HM(hf)	800	1.0	143.5	2,411 (176)
QTi13	H	800	1.0	264.0	1,697 (56)
QTi14	H	675	1.0	312.0	504 (167)
QTi15	H	725	1.0	168.0	711 (75)

[a]Symbols designating experiment types:
TZS titanite + zircon oxide mix with excess SiO_2 (hydrothermal)
H hydrothermal (quartz + rutile + zircon); Ag capsule
Other symbols as in Table 2

continuous nucleation during relatively slow cooling, or failure to equilibrate due to diffusive isolation (a rutile grain surrounded by a "barrier" phase having slow Ti diffusion kinetics or low Ti solubility might not maintain equilibrium with the bulk assemblage). Apart from their thin, Zr-rich rims and occasional ilmenite lamellae (see Appendix), the Labait rutiles are the most homogeneous of all the natural samples, probably because their host xenoliths cooled very quickly following eruption of the magma in which they were entrained.

Figure 6 reveals scatter in both the experimental and natural data that greatly exceeds analytical uncertainty, but the expected log(Zr) versus T^{-1} relationship is nevertheless borne out remarkably well over a total range in temperature of almost 1,000°C. A combined fit to all the data yields the following dependence of Zr content of rutile upon temperature:

$$\log(\mathrm{Zr}) = (7.36 \pm 0.10) - \frac{4470 \pm 120}{T(\mathrm{K})}, \qquad (8)$$

where the indicated uncertainties are at the 2-σ confidence level. In contrast to the situation with zircon, the experimental and natural calibrations agree within uncertainty. The combined experimental and natural data span a significant range in pressure: the experiments were conducted at 1.0–1.4 GPa (Table 4) and the natural rocks range from ~0.35 GPa for the greenschist (GS; Spear et al. 2002) to >3 GPa for the harzburgite vein rutiles (LB; Lee and Rudnick 1999). Despite these differences in crystallization pressure, all data conform reasonably well to a log(Zr) versus T^{-1} relation (Fig. 6). This fact, along with the absence of a discernible difference between the experimental and natural data sets, suggests that any effect of pressure is small over the range of conditions encountered in the Earth's crust. It is important to bear in mind, however, that the experimental portion of this study did not include large or systematic variations in pressure (see Comparison with other studies and the effect of pressure).

Rearranged to solve for temperature, Eq. (8) becomes

$$T\ (^{\circ}\mathrm{C})_{\mathrm{rutile}} = \frac{4470 \pm 120}{(7.36 \pm 0.10) - \log(\mathrm{Zr})} - 273. \qquad (9)$$

Figure 7 shows the absolute uncertainty, Δ T (2σ), as a function of T(C) for the combined 'natural + experimental' Zr-in-rutile thermometer. The curve at the top of the figure applies to the thermometer calibration itself, with no consideration of added uncertainty arising from analytical errors. In most instances, application of this thermometer to natural rocks will involve EMP analyses (as opposed to IMP analyses for Ti in zircon). Uncertainty in temperature estimates resulting from analytical uncertainty will be determined mainly by the level of Zr present, and to some extent by instrument settings and X-ray counting times; illustrative examples are shown in the lower panel of Fig. 7. The analytical uncertainty alone enters into characterization of relative temperatures or temperature changes.

Comparison with other studies and the effect of pressure

The thermometer expressed by Eqs. 8 and 9 is consistent to varying degrees with the two other Zr-in-rutile calibrations available at the present time. Zack et al. (2004) conducted a comprehensive study of Zr contents of rutile crystals in 29 metamorphic rocks for which major-phase thermobarometry was available. The authors focused upon rounded rutile grains included in (but not exolved from) garnet, believing that these would have coexisted with zircon (and quartz) during garnet growth at peak metamorphic conditions (In the present study, we used no specific criteria in choosing rutile grains for analysis, essentially selecting grains at random). Zack et al. (2004) presented their calibration in a form different from that of equation 9, expressing temperature as

Table 5 Zr contents of natural rutile crystals determined by electron microprobe (see text for analytical details and Appendix for sample descriptions)

ID	Description of analyses	ppm Zr (2 s.e.)
Stillup Tal aluminous schist (ST)		
xtl #1	4 pts., core and rim	90 (34)
2	12 pts. + traverse of 10	78 (14)
4	11 pts. + traverse of 13	114 (10)
5	5 pts., core and rim	117 (10)
7	3 pts. + traverse of 9	109 (10)
8	5 pts., core and rim	87 (12)
	Overall mean, 6 crystals	99 (13)
Labait harzburgite (LB)		
	R.L. Rudnick, personal communication	12,600 (600)
xtl #1	Traverse, 72 points	12,900 (90)[a]
2	Traverse, 52 points	13,300 (180)[a]
	Overall mean ($n = 132$)	12,900 (100)
Santa Catalina migmatite[b] (SC)		
xtl #1	MM1b, 5 random pts.	295 (90)
2	MM2b traverse, 9 pts.	429 (26)
3	RSTC, 3 random pts.	339 (121)
4	MM2b traverse, 6 pts.	168 (32)
5	MM1b, 12 random pts.	284 (36)
6	MM1b traverse, 10 pts.	234 (47)
7	MM1b traverse, 20 pts.	228 (24)
8	MM1b traverse, 15 pts.	175 (23)
	Overall mean, 8 crystals	269 (62)[a]
Vermont greenschist (GS)		
	8 sm. grains, 2 pts. each	37 (19)[c]
ID	Description of analyses	ppm Zr (2 s.e.)
Sifnos blueschist (SF)		
10 rock samples	60 rutile grains total; 6–12 analyses on each grain	25 (6)
Adirondack migmatite[d] (ADK)		
L1	Traverse, 25 pts.	1,833 (48)
L2	2 pts.	884 (57)
L3	1 pt.	1,610
L4	5 pts.	2,102 (136)
L5	5 pts.	676 (17)
L6	5 pts.	816 (84)
L7	4 pts.	1,411 (90)
L8	3 pts.	1,981 (89)
L9	3 pts.	1,838 (148)
L10	4 pts.	1,400 (90)
L11	2 pts.	747 (19)
L12	5 pts.	2,016 (108)
R1	4 pts.	2,111 (448)
R2	Traverse, 25 pts.	1,370 (20)
R3	Traverse, 13 pts.	1,896 (63)
R4	Traverse, 9 pts.	1,824 (18)
R5	Traverse, 13 pts.	605 (26)
R6	5 pts.	872 (124)
R7	2 pts.	1,210 (12)
	Overall mean (19 crystals)	1,432 (243)[c]

[a]These traverses were edited to remove points on Zr-enriched rims and occasional, thin exolution lamellae of Mg-ilmenite (see text)
[b]Sample identifiers (MM and RSTC) as in Sorensen and Grossman (1989)
[c]Variance is significantly greater than X-ray counting uncertainty (in general, intergrain σ > intragrain σ)
[d]*L* leucosome rutile; *R* restite rutile

$$T\ (^{\circ}\mathrm{C}) = 127.8 \times \ln(\mathrm{Zr}) - 10 \qquad (10)$$

where Zr is in ppm. This relation is shown in Fig. 8 (the "ZMK" curve) compared with the present result. The two calibrations cross at a temperature of ~540°C but diverge significantly at higher and lower temperatures: 300 ppm Zr, for example, corresponds to ~720°C by the ZMK thermometer and 640°C by the present (WWT) calibration; 20 ppm Zr corresponds to 373° and 464°, respectively, using the ZMK and WWT thermometers. The source of the divergence is unclear, but it seems possible that the emphasis Zack et al. (2004) placed upon rutile grains included in garnet and clinopyroxene (~2/3 of their data; see caption to their Table 3) may have influenced their empirical calibration. Zack et al. also note that "In general, rutile is best preserved as inclusions in garnet. The occurrence of such rutile inclusions in garnet has been applied as a key sample criteria [sic]. Special care was taken finding unaltered, rounded and monomineralic rutile grains surrounded by fresh garnet". As a consequence of the (commendable) care taken by Zack et al. in targeting specific rutile grains, it seems possible that the Zr contents of some rutile grains were affected by diffusive isolation from

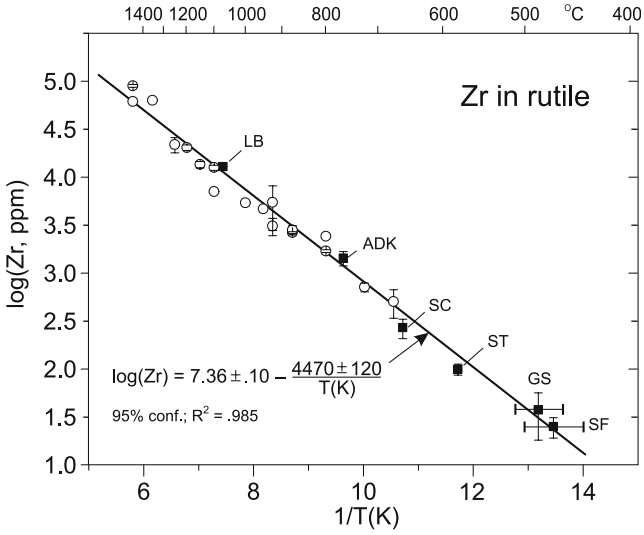

Fig. 6 Zr analyses of synthetic (*open circle*) and natural (*filled square*) rutile crystals plotted against $1/T$. The *heavy solid line* is the "global" fit to all data (independent fits to the experiments and natural data are not significantly different from one another or from the global fit). See text for explanation and discussion

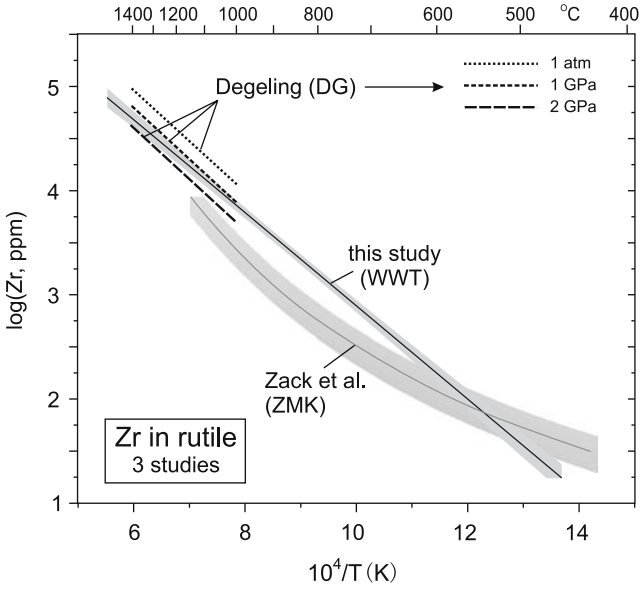

Fig. 8 Comparison of the three existing determinations of the Zr content of rutile (coexisting with zircon + quartz or siliceous melt) as a function of temperature. The calibration of Zack et al. (2004) is empirical and based on analyses of rutile grains in 29 rocks. Degeling (2003) made 31 experimental measurements spanning 1,000–1,500°C at 0.0001, 1.0 and 2.0 GPa, plus a single experiment at 1.600°C and 0.0001 GPa (forward and reversal experiments were conducted at 0.0001 and 1 GPa). The *lines* represent her preferred data set, from which thermodynamic parameters were derived (the 1,500 and 1,600°C data were excluded due to the presence of melt). The *shaded regions* represent confidence bands of the respective thermometers. See text for discussion

zircon. Alternatively, the substantial variations in equilibration pressure (~1–4.5 GPa) of the rutile grains examined by Zack et al. (2004) may have influenced

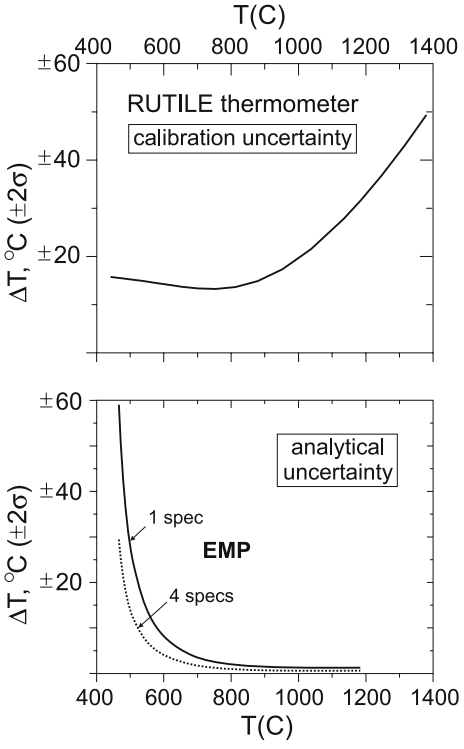

Fig. 7 Uncertainties in temperature estimates obtained using the Zr-in-rutile thermometer. *Top* 2-σ uncertainty inherent in the calibration itself, based on the least-squares fit to the combined experimental and natural data (Fig. 6; Eq. 8). *Bottom* Uncertainties resulting from EMP X-ray counting statistics. The EMP operating conditions and the significance of the uncertainties are the same as described in the caption to Fig. 5

their Zr values (see below). Whatever the reason for the differences between our results and those of Zack et al., our more indiscriminant choice of rutile grains resulted in natural data that are more consistent with the experimental results.

Our overall data set (experiments + natural samples) is in good agreement with experimental results reported by Degeling (2003), who measured Zr contents of rutile crystals coexisting with zircon and quartz (or SiO_2-rich melt) at 0.0001, 1.0 and 2.0 GPa and 1,000 to 1,500°C. As shown in Fig. 8, the Degeling (DG) calibration brackets our composite (experimental + natural) line over the temperature range where the two studies overlap: her 0.0001-GPa (1-atm) line lies above ours and her 2-GPa line slightly below; her 1-GPa line is nearly coincident with ours at 1,000°C but has a slightly steeper slope. For Degeling's preferred data set (shown in Fig. 8; see caption), the slopes of her three isobars are not statistically different. The two studies complement each other very well in the following respect: Degeling's (2003) data address the sensitivity of Zr uptake in rutile to variations in both temperature *and* pressure, but cover a somewhat restricted (high) temperature range. Our results span a very large temperature range, but we did not explore the effect of pressure in a systematic manner.

Degeling's (2003) study includes a detailed thermodynamic treatment of the effect of pressure on Zr uptake in rutile based on her experimental data. A practical discussion here might be helpful to potential users of the Zr-in-rutile thermometer. We take two approaches to bracket the magnitude of the pressure effect as it might bear on rocks formed at $T < 1{,}000$°C in the 1–2 GPa range (this deliberately excludes discussion of ultra high-pressure metamorphic rocks because this would require extrapolations well beyond the experimental calibration range). The first approach is to assume that the slope of the line in Fig. 6 describes the temperature dependence of Zr uptake in rutile at both 1 and 2 GPa. This slope is about 3% shallower than the average of Degeling's three isobars (0.0001, 1 and 2 GPa; see Fig. 8), which are not statistically different from one another. However, our slope might be considered as more 'accurate' because of the large range in $1/T$ space covered by our data. We regressed lines having the slope from Fig. 6 through Degeling's data at 1 and 2 GPa in order to extrapolate to temperatures well below those represented by her data. The implications are shown in Fig. 9 as a plot of the temperature underestimate (ΔT) that would result from using our nominally 1-GPa thermometer on a rock that actually equilibrated at 2 GPa. The deviation ranges from ~26° at an apparent temperature of 500 to ~90°C at 1,100°C.

A second approach to evaluating the effect of pressure at $T < 1{,}000$°C is to extend Degeling's results using the expected thermodynamic dependence of Zr content upon both temperature and pressure. This approach must assume that both ΔH and ΔV of the relevant ZrO_2 exchange reaction are constant over the range of conditions considered. Down-temperature extrapolation at 1 and 2 GPa using Degeling's (2003) data and her calculated thermodynamic parameters reveals that a temperature of 500°C returned by our ~1-GPa thermometer would under-represent the actual temperature of a 2-GPa rock by ~51°. For an apparent temperature of 1,100°C, the underestimate would be ~90° (see Fig. 9). This latter approach is thermodynamically sound, but it also necessitates assumptions (constancy of ΔH and ΔV) that—although certainly allowed by Degeling's high-temperature data—cannot be confirmed given the experimental uncertainty. The thermodynamic treatment predicts a slight divergence of the log(Zr) versus T^{-1} isobars (1 and 2 GPa) that can be neither confirmed nor ruled out by our data for reasons discussed in the next paragraph.

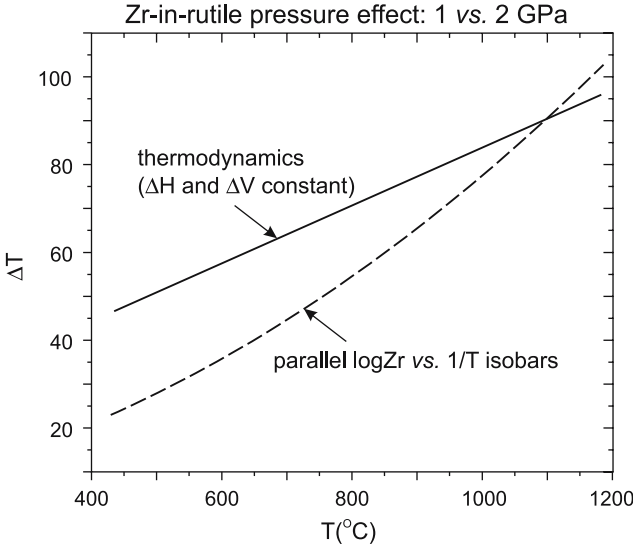

Fig. 9 Estimated effect on the Zr-in-rutile thermometer of increasing pressure from 1 to 2 GPa. ΔT is the amount by which the temperature of rutile growth would be underestimated by applying our nominally 1-GPa Zr thermometer (Fig. 6) to a rutile crystal that actually grew at 2 GPa. Two different approaches are used: one based on the form of the P- and T-dependencies expected from thermodynamics (*solid line*), the other upon the assumption that a 2-GPa isobar would parallel the line in Fig. 6 (*dashed line*). See text for more discussion

Circumstantial evidence from the natural rocks we examined can be used, cautiously, to argue that the pressure effect is modest over the range of pressures encountered in most crustal systems. First, the Zr-in-rutile temperatures returned by our experimentally calibrated thermometer (corresponding to ~1 GPa) for the Sifnos blueschist (SF) and Vermont greenschist (GS) are consistent with other temperature estimates for these rocks even though the pressures deviate significantly from 1 GPa in both directions (1.5 and 0.35 GPa, respectively). This consistency is of limited value, however, because both the Zr analyses and the independent temperature estimates for these two rocks carry substantial uncertainties. It is tempting to regard the coincidence in Zr content of the ~3-GPa LB rutiles with that predicted by our 1-GPa experimental calibration as proof of a very minor pressure effect on Zr uptake. In this case, however, it must be borne in mind that the Labait assemblage lacks quartz, so the ZrO_2 activity is unbuffered and potentially higher than in the quartz-present case. The apparent agreement between ~3- and ~1-GPa data may thus be due to fortuitously compensating variables—that is, increased pressure suppressing Zr uptake and increased ZrO_2 activity enhancing it. A more complete understanding of the effect of pressure on the Zr-in-rutile thermometer will surely develop as future data are acquired from both natural systems and experiments. Some of the differences between our Zr-in-rutile calibration and that of Zack et al. (2004) may ultimately be attributed to a pressure effect.

Diffusion issues: preview of new data for Zr in rutile and speculations on Ti in zircon

A question that arises in the application of any geothermometer is the resistance of recorded temperatures to diffusive re-equilibration. In some instances, a response to changing temperature is desirable because it creates the potential for determining temperature-time

paths; in other instances, however, the hope is that a record of peak conditions will be preserved through the retrograde cycle.

As noted in Results of this study, the rutile crystals in some of the natural rocks investigated in this study show significant inter-grain variability in Zr content. The variances (error bars) appear relatively small on the log scale of Fig. 6, but the analyses of individual grains (Table 5) paint a somewhat different picture, especially for the SC and Adirondack samples. The source of the variance is uncertain, but partial diffusive re-setting of Zr content in response to changing temperature is one possibility. Manchester et al. (2006) have characterized diffusion of Zr and Hf in rutile, which are described by the following Arrhenius relations

$$D_{Zr}^{//c} = 9.77 \times 10^{-15} \exp\left(\frac{-171{,}000}{RT}\right)$$
$$D_{Hf}^{//c} = 9.12 \times 10^{-15} \exp\left(\frac{-169{,}000}{RT}\right)$$
$$D_{Hf}^{\perp c} = 2.51 \times 10^{-12} \exp\left(\frac{-227{,}000}{RT}\right),$$

where the diffusivities (D) are in m^2/s and the activation energies in J/mol. Diffusion of Zr was not characterized perpendicular to the c crystallographic direction, but the diffusivities of Zr and Hf are nearly identical parallel to c, so Zr diffusion $\perp c$ is inferred to be the same as Hf $\perp c$. The diffusivities given by these equations do indeed point to possible open-system behavior under some metamorphic conditions. For rutile grains of 500 μm radius, the Dodson (1973) closure temperatures (T_C) are ~670°, 770°, and 890° for cooling at 1°, 10° and 100°/m.y. For grains of 100 μm radius, (T_C) is ~560°, 635°, and 730°, respectively, for the same set of cooling rates [Note: At temperatures below ~1,000°C, diffusion is faster // c than $\perp c$, so c-parallel diffusivities were used in calculating (T_C). In the case of needle-shaped rutile crystals, this choice might not be appropriate]. Zirconium diffusion is clearly fast enough to compromise recorded high temperatures in some cases, but local circumstances (e.g., the nature of bounding phases and/or the efficiency of grain-boundary transport) may lead to local Zr retention even during slow cooling. Exolution of baddeleyite from the rutile lattice (possibly followed by reaction with nearby quartz to form zircon) is another possible response of a high-Zr rutile grain to cooling (Degeling 2003; Bingen et al. 2001).

At the time of this writing, no data have been published for Ti diffusion in zircon, but a few observations are nonetheless warranted. Arrhenius relations are available for diffusion of several tetravalent cations (U^{4+}, Th^{4+}, Hf^{4+}; Cherniak et al. 1997a) in non-metamict zircon, and the diffusivities at crustal conditions are exceedingly low: at 900°C, the characteristic diffusion distance for these ions is 10–20 nm in a billion years. The pre-exponential factor, D_o, depends systematically upon ionic radius, which results in a factor of ~5 higher diffusivity for Hf relative to U and Th (Hf^{4+} is ~20% smaller). Extrapolation of the established size dependence to the still smaller Ti^{4+} ion suggests a diffusivity ~3× higher than that of Hf, but this is a marginally significant difference: Ti diffusion is still predicted to be negligible for all plausible geologic conditions. This preliminary analysis raises the interesting possibility that the crystallization temperature recorded by the incorporation of Ti in zircon is more robust than the radiometric age (because predicted Ti diffusivities are much lower than measured values for Pb and REE; see Cherniak and Watson 2001; Cherniak et al. 1997b). Experimental information is now available to substantiate the low diffusivity estimate for Ti in zircon. Cherniak and Watson (in preparation) have determined a preliminary value of $4\times10^{-22} m^2/s$ at 1,400°C, which is only slightly higher than the above estimate based on 4+ ion systematics. The activation energy for Ti diffusion is still unconstrained, but a reasonable choice based on diffusion systematics of other tetravalent cations (Cherniak et al. 1997a) implies immeasurably slow Ti diffusion in non-metamict zircon under most geologic conditions.

Zircon thermometry of selected rocks

During the course of this project, ion-microprobe analyses of zircons from five localities were obtained that are not included Table 3 or Fig. 4, generally because the crystallization temperatures and circumstances were too poorly constrained for use in the thermometer calibration. These can now be discussed briefly in the context of the thermometer.

Hadean zircons Titanium analyses of 54 Hadean zircons from Western Australia's Jack Hills—perhaps the most compelling target of the Ti-in-zircon thermometer—yield crystallization temperatures that cluster strongly at ~700°C (Watson and Harrison 2005). This result implies a dominant wet crustal melting origin for the growth media of these zircons, adding credence to earlier suggestions that the Hadean Earth was "cool and wet" (Mojzsis et al. 2001; Wilde et al. 2001). A few of the Hadean zircons analyzed by Watson and Harrison returned temperatures in excess of 750°C, indicating occasional crystallization in alternative settings (e.g., mafic intrusions; see Skaergaard results below).

Honeycomb Hills (HCH) topaz rhyolite Zircons from this F-rich, low-T rhyolite (Byrd and Nash 1993; samples courtesy of B. Nash) were examined in the hope of including a low-T, igneous zircon in the Ti versus T calibration. HCH zircons are generally small and chemically complex: most contain what appear in CL to be inherited cores, and many have truncated zoning features ("unconformities"). The lowest Ti concentrations (1.4–1.6 ppm) were obtained by the "polished-facet" approach (see Analysis of natural zircons and rutiles: strategies and complications); these represent the

outermost rims of the crystals and are probably the best measurable indication of the eruption temperature. The HCH rhyolite is not saturated in rutile or any other titanate phase, so a_{TiO_2} must be estimated by the method described for the BT (Zircon) in order to estimate the crystallization temperature of the zircons. The Ti contents of the majority of quartz phenocrysts indicate $a_{TiO_2} \sim 0.36$, so the Ti content of the zircon rims implies a crystallization temperature of ~670°C. This is lower than the eruption temperature of a typical rhyolite (e.g., the BT), but not as low as expected for these halogen-rich eruptive pegmatites (Congdon and Nash 1991; Byrd and Nash 1993). The disagreement may arise because of the difficulty in characterizing the Ti concentration at the outermost surface of the zircons. The mass of zircon that can be crystallized by a low-*T*, siliceous melt over a 50°–100° temperature drop is limited by the very low solubility of zircon—only about 10 ppm Zr at 600°C (Watson and Harrison 1983). Moreover, a given zircon may not add mass uniformly to all surfaces during cooling. "Clean" analyses of low-T zircon may require careful IMP depth profiling of several crystal facets.

Skaergaard mafic intrusion, eastern Greenland Three lath-shaped zircons from the late differentiates ("sandwich horizon") of the Skaergaard intrusion (courtesy of M. Hamilton) returned temperatures of 787–806°C. These results may underestimate the actual crystallization temperatures due to undersaturation of the system in rutile, but the temperatures are not unreasonable given the estimated ~870°C average saturation temperature of the Skaergaard late differentiates in zircon [as determined by application of the zircon saturation thermometer (Watson and Harrison 1983) to appropriate melt compositions (Brooks 1969; Wager and Brown 1968)], and the 950–980°C estimate for late-stage crystallization of the Skaergaard magma (Lindsley et al. 1969).

Ultramafic xenoliths, Highwood Mountains, Montana Zircons separated from a harzburgite xenolith and cross-cutting glimmerite vein from the Highwood Mountains (samples EN88H-3 and EN88-V; Rudnick et al. 1999) returned temperatures broadly consistent with the 600–700°C estimate from major-phase thermometry. The harzburgite zircons appear to have crystallized over a relatively narrow range in temperature ($\bar{x} = 760°C; \sigma = 30; n = 8$), while those associated with the vein material crystallized over a lower and much broader temperature range ($\bar{x} = 700°C; \sigma = 111; n = 6$). One of these vein zircons yielded the lowest temperature yet returned by the Ti-in-zircon thermometer: 545°C [which is clearly subject to some uncertainty (Fig. 5)]. Our original intent in analyzing these mantle zircons had been to include them in the thermometer calibration itself. In the end we elected not to do so: even though the agreement with prior temperature estimates is reasonably good, the major-phase thermometry does not provide tight constraints on temperature, and coexistence of the zircons with rutile is uncertain. The harzburgite contains Mg-ilmenite, and rutile is locally present in some glimmerite veins (Rudnick et al. 1999), but the zircons we analyzed (kindly provided by R.L. Rudnick) had already been separated from their host rocks. The consistency of the Highwood Mountains results with the Ti thermometer is satisfying, but also leads to the interesting realization that some shallow-mantle zircons may crystallize at temperatures typical of wet granitoid-derived zircons. To a first approximation, the Highwood Mountains zircons return Ti temperatures similar to those of the Hadean zircons; however, the Jack Hills samples are clearly distinguished as crustal and "granitoid" on other grounds (Maas et al. 1992; Mojzsis et al. 2001; Wilde et al. 2001; Trail et al. 2004).

Isotope standard 91500 During the course of this study, interlaboratory zircon standard 91500 (Wiedenbeck et al. 1995) was repeatedly analyzed for Ti using the IMP calibration based on zircons from experimental runs 57 and 59 and a Ti-free synthetic sample (see Ion microprobe (IMP): general operating conditions). The 91500 fragment in the standard collection at the Woods Hole ion-probe facility contains relatively little Ti and is not sufficiently homogenous to serve as stand-alone IMP or LA-ICP-MS standard for Ti. However, the 3–6 ppm we consistently measured—corresponding to a nominal crystallization temperature of ~650–700°C—is not inconsistent with the paragenesis of the 91500 zircon in a titanite-bearing syenitic pegmatite.

Concluding remarks: application considerations

For reasons noted in the introduction, the thermometers presented in this paper have numerous potential applications, but both have limitations as well. Those surrounding the Zr-in-rutile thermometer are discussed first because they are simpler.

Zirconium contents of rutiles crystallized above ~500°C can be determined easily by EMP, and the excellent spatial resolution of this venerable analytical technique will allow characterization of intracrystalline variations through traverses and X-ray mapping. As noted by Zack et al. (2004), secondary fluorescence may contribute to analyses of small rutile grains, and in no case would this problem be more severe than in the analysis of small rutile inclusions in zircons [rutile inclusions in both Hadean (Trail et al. 2004) and "modern" zircons are an obvious target for rutile thermometry]. Even though the Zr contents of rutile grains included in zircons will often be well above MDL with the EMP, the ion microprobe (or nano-SIMS) may be necessary to obtain clean in situ analyses. For applications involving temperatures below ~450°C, the IMP or

LA-ICP-MS will generally be necessary for determination of Zr contents, and in this case small crystal sizes may pose problems. Because of the relatively rapid diffusion of Zr in rutile (see Diffusion issues: preview of new data for Zr in rutile and speculations on Ti in zircon), the possibility of diffusive re-setting in higher-temperature systems may complicate interpretation of apparent temperatures and zoning profiles.

For Ti analysis of zircons, an ion probe or LA-ICP-MS will be required in all but the highest-T cases, and this will introduce challenges with respect to spatial resolution, especially when new growth is limited to thin rims and crystal tips. Sputtering into the surfaces with the ion probe may be required in some cases. An additional potential drawback of zircon Ti thermometry not unrelated to the spatial resolution issue is that preservation of inherited temperatures will be common because zircon itself is so durable and Ti diffusion is probably so slow (Diffusion issues: preview of new data for Zr in rutile and speculations on Ti in zircon). We saw ample evidence of "temperature inheritance" in the Adirondack, ST and Honeycomb Hills zircons.

In closing, we call attention to two analytical problems encountered in determining Ti content of zircon by IMP in addition to the $^{96}Zr^{2+}$ interference already noted. A minor but ubiquitous problem is that the Au coat applied at the Wood Hole ion-probe facility contains a small amount of Ti (~1 ppm). Adequate surface preparation with the ion beam prior to counting Ti addresses this problem satisfactorily at the concentration levels relevant to this study, but the issue may be more problematic in the case of very low-Ti (e.g., hydrothermal) zircons. The second problem is that the reddish-brown oxide coating on zircons that have endured a sedimentary environment contains high concentrations of Ti. This coating is not necessarily limited to the outer surfaces of the zircons, but may also penetrate into cracks. Consequently, any overlap of the primary ion beam onto cracks and outer surfaces can lead to erroneously high apparent Ti concentrations in target zircons. This problem was occasionally evident in the case of the Jack Hills zircons, many of which are coated with iron oxide/hydroxide. In severely cracked zircons, a clean ion-probe analysis may not be possible, but suspiciously high Ti contents can be confirmed or discredited by EMP even if the actual low level (<10 ppm) cannot be determined.

Acknowledgements A great many people helped to make this work possible. The following individuals graciously provided the samples reported on in this study: E. Baxter (Stillup Tal), M. Hamilton (Skaergaard), B. McDonough, B. Nash, R. Rudnick, S. Sorensen, F. Spear and L. Storm. The following individuals also generously complied with our requests for zircons and rock samples: J. Hanchar, A. Irving, D. Lindsey, R. Kerrich, D. London, G. Pearson, T. Pettke, M. Picard (Canadian Museum of Nature), and D. Rumble. In the end, zircons and rutiles in most of these latter samples were not analyzed because the rocks did not meet the criteria required for inclusion in thermometer calibrations: namely, independently constrained temperature, known or calculable activities of relevant components, and reasonable evidence for lack of inheritance in analyzable portions of the zircons. The analytical aspects of the project were expedited immeasurably by Graham Layne (IMP protocols for Ti in zircons) and also by Lara Storm and Frank Spear, who allowed us to use their unpublished data on Zr in natural rutiles (ADK and SF, respectively). During the course of the project, we benefited from extensive discussions with Daniele Cherniak, Mark Harrison, Joe Pyle, Frank Spear, Lara Storm and Dustin Trail. Helen Tomkins (née Degeling) generously provided access to her unpublished data and contributed significantly to our thinking about the effect of pressure on the Zr-in-rutile thermometer. The manuscript was improved significantly by the critical reviews of Thomas Zack and an anonymous reviewer. This work was supported by the Earth Sciences Division of the National Science Foundation, through grants EAR 0073752 and EAR 0440228 to EBW.

Appendix

Natural rocks: sample descriptions and temperatures of zircon and rutile growth

Our knowledge of the growth temperatures of zircon and rutile crystals in the natural rocks is dependent upon temperature estimates obtained by other means, in most cases by other workers. We must assume, in addition, that the zircons and rutiles did in fact grow at these estimated temperatures. For the metamorphic rocks, we generally assume that the rutile and zircon crystals we examined grew simultaneously at peak conditions and that their compositions did not change during cooling (this assumption seems well founded for zircon, less so for rutile in some cases; see below and Diffusion issues: preview of new data for Zr in rutile and speculations on Ti in zircon of main text).

Bishop tuff (725°C) The BT rhyolitic magma has been the target of several detailed investigations (e.g.,

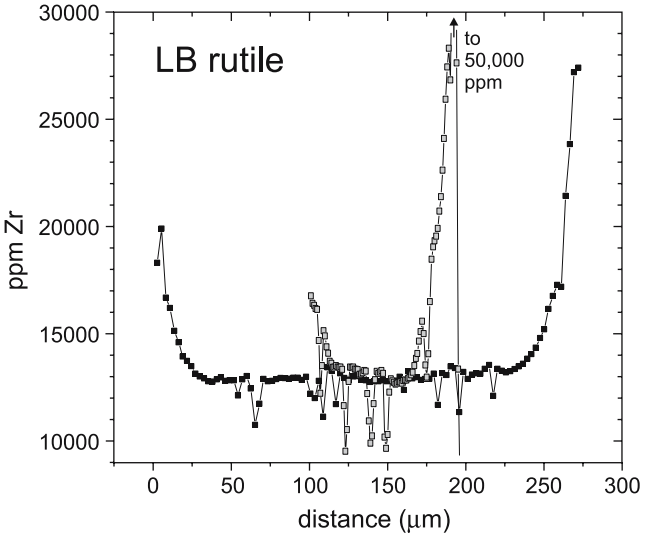

Fig. 10 Rim-to-rim electron microprobe scans across two rutile grains in the Labait harzburgite. The "background" level of ~13,000 ppm is used in the Zr-in-rutile thermometer. Note the consistent enrichment in Zr near the grain margins, probably caused by pre-eruptive heating that caused "in-diffusion" of Zr from nearby zircons. The negative "spikes" in Zr content are exolved ilmenite lamellae. See text and Appendix for discussion

Hildreth 1979; Anderson et al. 2000), so sample descriptions are not needed here. Moreover, because the BT magma was not saturated in rutile, the assigned zircon crystallization temperature (725°C) is addressed in the main text (Zircon). As noted, we ignore the apparent late heating event recorded by Ti in quartz phenocrysts (Wark et al. 2004), because zircon would likely dissolve slightly during this event, and because the capacity of a magma to crystallize zircon at this late stage is exceedingly small due to the low solubility (Watson and Harrison 1983).

Labait harzburgite (1,070°C) The zircon and rutile in this harzburgite are found in diffuse metasomatic veins with phlogopite, orthopyroxene, olivine, chromite and sulfides (Rudnick et al. 1999; Lee and Rudnick 1999). The crystallization temperature of 1,070°C reported by Lee and Rudnick (1999) is based on the two-pyroxene thermometer of Brey and Köhler (1990) and the CaO-in-orthopyroxene thermometer, also of Brey and Köhler (1990). As noted in Zircon, the LB probably experienced a brief, late heating event immediately prior to eruption. The existence of such an event is implied by the high-Ca rims on orthopyroxene noted by Lee and Rudnick (1999); the zircons and rutiles we analyzed shown corroborating evidence. The zircons have locally high Ti abundances (up to ~800 ppm) in patches near the grain margins, and the rutiles exhibit continuous, high-Ti rims suggesting diffusive uptake of Zr in response to increased T (see Fig. A1). The inferred late heating event does not appear to have affected the spatially dominant interiors of the zircon and rutile crystals, which are quite uniform in their Ti and Zr contents, respectively (see Tables 3, 5, Fig. 10). It is these broad interior regions that are assumed to have formed at 1,070°C. The LB is estimated to have equilibrated at P~3.0 GPa on the basis of the low Al_2O_3 content of orthopyroxene (Lee and Rudnick 1999).

Adirondack migmatite (765°C) Zircons and rutile crystals analyzed in this study were separated from two samples of a migmatitic metapelite outcrop in the southern Adirondack Highlands of New York State, USA (43° 14.630′N; 74° 19.732′W), designated ADK-01-6A and ADK-01-6B by Storm and Spear (2005). The major-phase assemblage is garnet + biotite + plagioclase + alkali-feldspar + quartz + sillimanite. Leucosome material dominates the outcrop, but dispersed restitic portions remain. Rutile grains from both leucosome and restite were analyzed for Zr (Table 5); all zircons came from the leucosome. Storm and Spear (2005) used garnet-biotite thermometry and GASP barometry to estimate peak P–T conditions of at least 790°C and 0.7–0.9 GPa. If biotite reacted out completely during progressive heating, the peak temperature may have been as high as 820°C. Storm and Spear (2005) placed the solidus at ~740°C, which means that the system experienced a melt-present interval of at least ~50°C. We assumed that the rutile crystals and the CL-dark rims on the zircons (Fig. 3) grew during cooling from a peak temperature of ~790°C down to the solidus at ~740°C; the 765°C midpoint was used for plotting purposes. The range in Ti content of the zircon rims may reflect real temperature variation over the growth interval, but the ion probe lacks the spatial resolution needed to systematically traverse the rims. Zoning of rutile with respect to Zr is not systematic, and the concentration differences among grains are larger than those within individual grains (see Table 5 and main text for discussion).

Stillup Tal aluminous schist (580°C) This sample is from a shear zone through a granodiorite in which the rocks have been transformed into aluminous schist through extensive fluid–rock interaction. Our zircon + rutile separate was recovered from the biotite–phengite schist (zone III) described by Selverstone et al. (1991), who determined the P–T history of adjacent garnet-bearing rocks (zones I, II and IV) using garnet–biotite thermometry and garnet-plagioclase-muscovite-biotite barometry. The garnet–mica schists of zones II and IV recorded final equilibration conditions of 540–575°C and 0.7–0.8 GPa; zone I indicated slightly higher temperatures of 570–610°C. Lacking better constraints, we chose to plot our zircon and rutile information at 580°C.

Sifnos blueschist (470°C) Metabasites and metapelites of Sifnos (Cycladic Islands), Greece preserve high-pressure assemblages from an Eocene (40 Ma) metamorphic event. The rutile grains analyzed for Zr in this study occur in both mafic and pelitic hosts, and are assumed to have grown at 470 ± 30°C, an estimate based on garnet–omphacite geothermometry by Schliestedt (1986). The equilibration pressure is estimated to have been 1.5 ± 0.3 GPa. See Spear et al. (2006) for additional discussion.

Vermont greenschist (485°C) This sample is from the eastern Vermont metamorphic belt near Bellows Falls, Vermont (USA) and contains the major-phase assemblage garnet + biotite + chlorite + muscovite + plagioclase + quartz. Accessory rutile occurs in small (up to ~300 μm), generally anhedral intergrowths with ilmenite. The P–T history of the rocks in this region has been determined using a variety of approaches, including thermobarometry, garnet zoning analysis, pseudomorph textures, and placement on petrogenetic grids, as summarized by Spear et al. (2002). The equilibration pressure of this sample is estimated to be 0.35 ± 0.03 GPa.

Santa Catalina migmatite (660°C) The rutiles and zircons analyzed are from the MM-RST suite of migmatites described by Sorensen and Grossman (1989). These migmatites occur as blocks in the upper part of the Catalina amphibolite unit, which is part of blueschist-bearing Cretaceous subduction complex. The migmatites represent the most altered lithologies of a

probable metabasalt protolith, and contain (in addition to zircon and rutile) the assemblage garnet + hornblende + plagioclase + quartz + (minor) zoisite, clinozoisite, allanite, apatite ± muscovite ± (minor) titanite, kyanite and chlorite. The migmatites are believed to be the result of melting in the presence of low-salinity aqueous fluid (Sorensen and Barton 1987). Rutile and zircon crystals were sufficiently large and abundant to analyze in situ (i.e., without performing separations) by EMP and IMP, respectively, in thin sections generously provided by S. Sorensen. Sorensen and co-workers place the P–T conditions of migmatite formation at 0.8–1.1 GPa and 640–750°C, but were unable to narrow the temperature estimate any further. In this instance, we chose to narrow the range ourselves. We considered the zircons and rutiles to have crystallized near the lower end of this range (660°C) because this is much more consistent with the Zr contents of the rutiles. It is worth noting, also, that the water-saturated solidus of these rocks at 1 GPa is ~650°C (Wyllie 1983; Johannes 1985). Our choice involves some circular reasoning—i.e., choosing a crystallization temperature for rutiles that are then included in the thermometer calibration—but this choice maximizes the consistency between the temperature range of Sorensen and co-workers and the temperatures indicated by the Zr content(s) of rutile and the Ti content(s) of zircon. As noted in the text, it is probable that rutile and zircon in most of the rocks studied co-crystallized over a range in temperature reflected by the ranges in Zr and Ti contents.

References

Anderson AT, Davis AM, Lu F (2000) Evolution of the Bishop Tuff rhyolitic magma based on melt and magnetite inclusions and zoned phenocrysts. J Petrol 41:449–473

Belousova EA, Griffin WL, O'Reilly SY, Fisher NJ (2002) Igneous zircon: trace element composition as an indicator of source rock type. Contrib Mineral Petrol 143:602–622

Bingen B, Austrheim H, Whitehouse M (2001) Ilmenite as a source for zirconium during high-grade metamorphism? Textural evidence from the Caledonides of western Norway and implications for zircon geochronology. J Petrol 42:355–375

Brey G, Köhler T (1990) Geothermobarometry in four-phase lherzolites II: new thermobarometers, and practical assessment of existing thermobarometers. J Petrol 31:1353–1378

Brooks CK (1969) On the distribution of zirconium and hafnium in the Skaergaard intrusion, East Greenland. Geochim Cosmochim Acta 33:357–370

Byrd BJ, Nash WP (1993) Eruption of rhyolite at the Honeycomb Hills, Utah—cyclical tapping of a zoned silicic magma reservoir. J Geophys Res 98:14075–14090

Cherniak DJ, Watson EB (2001) Pb diffusion in zircon. Chem Geol 172:5–24

Cherniak DJ, Hanchar JM, Watson EB (1997a) Diffusion of tetravalent cations in zircon. Contrib Mineral Petrol 127:383–390

Cherniak DJ, Hanchar JM, Watson EB (1997b) Rare-earth diffusion in zircon. Chem Geol 134:289–301

Compston W, Williams IS, Meyer C (1984) U–Pb geochronology of zircons from lunar breccia 73217 using a sensitive high mass-resolution ion microprobe. J Geophys Res Suppl 89:B525–B534

Congdon RD, Nash WP (1991) Eruptive pegmatite magma: rhyolite of the Honeycomb Hills, Utah. Am Mineral 76:1261–1278

Davis WJ (1997) U–Pb zircon and rutile ages from granulite xenoliths in the Slave province: evidence for mafic magmatism in the lower crust coincident with Proterozoic dike swarms. Geology 25:343–346

Davis GL, Krogh TE, Erlank AJ (1976) The ages of zircons from kimberlites from South Africa. Carnegie Inst Wash Yrbk 75:821–824

Degeling HS (2003) Zr equilibria in metamorphic rocks. Unpublished PhD Thesis, Australian National University, 231 pp

Dodson MH (1973) Closure temperature in cooling geochronological and petrological systems. Contrib Mineral Petrol 40:259–274

Dunbar NW, Hervig RL (1992) Petrogenesis and volatile stratigraphy of the Bishop tuff—evidence from melt inclusion analysis. J Geophys Res 97:15129–15150

Ghent ED, Stout MZ (1984) TiO_2 activity in metamorphosed pelitic and basic rocks—principles and applications to metamorphism in southeastern Canadian cordillera. Contrib Mineral Petrol 86:248–255

Harrison TM, Aikman A, Holden P, Walker AM, McFarlane C, Rubatto D, Watson EB (2005) Testing the Ti-in-zircon thermometer. Eos Trans AGU (program and abstracts, fall meeting 2005)

Hayden LA, Watson EB, Wark DA (2006) Rutile saturation in hydrous, siliceous melts and its bearing on Ti thermometry of quartz and zircon (in preparation)

Hayden LA, Watson EB, Wark DA (2005) Rutile saturation and TiO_2 diffusion in hydrous siliceous melts. Eos Trans AGU (program and abstracts, fall meeting 2005)

Hildreth W (1979) The Bishop Tuff: evidence for the origin of the compositional zonation in silicic magma chambers. Geol Soc Am Spec Paper 180:43–76

Hoskin PWO, Schaltegger U (2003) The composition of zircon and igneous and metamorphic petrogenesis. In: Hanchar JM, Hoskin PWO (eds) Zircon Rev Mineral Geochem, vol 53. Mineral Soc Am, Washington, pp 27–62

Ireland TR, Wlotzska F (1992) The oldest zircons in the solar system. Earth Planet Sci Lett 109:1–10

Johannes W (1985) The significance of experimental studies for the formation of migmatites. In: Ashworth JR (ed) Migmatites. Chapman and Hall, New York, Blackie, Glasgow, London, pp 36–86

Kennedy GC, Heard HC, Wasserburg GJ, Newton RC (1962) The upper 3-phase region in the system SiO_2-H_2O. Am J Sci 260:501–521

Kerrich R, King R (1993) Hydrothermal zircon and baddeleyite in Val-d'Or Archean mesothermal gold deposits—characteristics, compositions, and fluid-inclusion properties, with implications for timing of primary gold mineralization. Can J Earth Sci 30:2334–2351

Lee C-T, Rudnick RL (1999) Compositionally stratified cratonic lithosphere: petrology and geochemistry of peridotite xenoliths from the Labait Volcano, Tanzania. In: Gurney JJ, Richardson SR (eds) Proceedngs of seventh international kimberlite conference, Cape Town, South Africa, pp 503–521

Lindsley DH, Brown GM, Muir ID (1969) Conditions of the ferrowollastonite-ferrohedenbergite inversion in the Skaergaard intrusion, East Greenland. Mineral Soc Am Spec Paper 2:193–201

Maas R, Kinny PD, Williams IS, Froude DO, Compston W (1992) The Earth's oldest known crust: a geochronological and geochemical study of 3900–4200 Ma old zircons from Mt. Narryer and Jack Hills, Western Australia. Geochim Cosmochim Acta 56:1281–1300

Manchester JE, Cherniak DJ, Watson EB (2006) Diffusion of Zr and Hf in rutile (in preparation)

Mezger K, Hanson GN, Bohlen SR (1989) High-precision U–Pb ages of metamorphic rutile: applications to the cooling history of high-grade terranes. Earth Planet Sci Lett 96:106–118

Mezger K, Rawnsley C, Bohlen SR, Hanson G (1991) U-Pb garnet, sphene, monazite and rutile ages: implications for the duration of high-grade metamorphism and cooling histories, Adirondack Mountains, New York. J Geol 99:415–428

Mojzsis SJ, Harrison TM, Pidgeon RT (2001) Oxygen-isotope evidence from ancient zircons for liquid water at the Earth's surface 4300 Myr ago. Nature 409:178–181

Peppard BT, Steele IM, Davis AM, Wallace PJ, Anderson AT (2001) Zoned quartz phenocrysts from the rhyolitic Bishop tuff. Am Mineral 86:1034–1052

Rudnick RL, Ireland TR, Gehrels G, Irving AJ, Chesley JT, Hanchar JM (1999) In: Gurney JJ, Richardson SR (eds) Proceedings of seventh international kimberlite conference, Cape Town, South Africa, pp 728–735

Ryerson FJ, Watson EB (1987) Rutile saturation in magmas: implications for Ti-Nb-Ta depletion in island-arc basalts. Earth Planet Sci Lett 86:225–239

Schliestedt M (1986) Eclogite-blueschist relationships as evidenced by mineral equilibria in the high-pressure metabasic rocks of Sifnos (Cycladic Islands), Greece. J Petrol 27:1437–1459

Selverstone J, Morteani G, Staude J-M (1991) Fluid channelling during ductile shearing: transformation of granodiorite into aluminous schist in the Tauern Window, Eastern Alps. J Metamorph Geol 9:419–431

Sorensen SS, Barton MD (1987) Metasomatism and partial melting in a subduction complex: Catalina schist, southern California. Geology 15:115–118

Sorensen SS, Grossman JN (1989) Enrichment of trace elements in garnet amphibolites from a paleo-subduction zone: Catalina Schist, southern California. Geochim Cosmochim Acta 53:3155–3177

Spear FS, Kohn MJ, Cheney JT, Florence F (2002) Metamorphic, thermal and tectonic evolution of central New England. J Petrol 43:2097–2120

Spear FS, Wark DA, Cheney JT, Schumacher J, Watson EB (2006) Zr-in-rutile thermometry of blueschists from Sifnos, Greece. Contrib Mineral Petrol (submitted)

Speer JA (1982) Zircon. In: Ribbe PH (ed) Orthosilicates Rev Mineral, vol 5. Mineral Soc Am, Washington, pp 67–112

Storm LC, Spear FS (2005) Pressure, temperature and cooling rates of granulite facies migmatitic pelites from the southern Adirondack Highlands, New York. J Metamorph Geol 23:107–130

Trail D, Mojzsis SJ, Harrison TM (2004) Inclusion mineralogy of pre-4.0 Ga zircons from Jack Hills, Western Australia: a progress report. Geochim Cosmochim Acta 68(Goldschmidt Conf Abstr):A743

Turner G, Harrison TM, Holland G, Mojzsis SJ, Gilmour J (2004) Extinct ^{244}Pu in ancient zircons. Science 306:89–91

Wager LR, Brown GM (1968) Layered igneous rocks. Oliver and Boyd, Edinburgh

Wallace PJ, Anderson AT, Davis AM (1999) Gradients in H_2O, CO_2 and exsolved gas in a large-volume silicic magma system: interpreting the record preserved in melt inclusions from the Bishop Tuff. J Geophys Res 104:20097–20122

Wark DA, Watson EB (2004) Launching the TITANiQ: a titanium-in-quartz thermometer. Geochim Cosmochim Acta 68(Goldschmidt Conf Abstr):A543

Wark DA, Anderson AT, Watson EB (2004) Probing Ti in Quartz: application of the TITANiQ thermometer to the Bishop Tuff. EOS Trans Am Geophys Union (joint assembly program and abstracts)

Watson EB, Harrison TM (1983) Zircon saturation revisited: temperature and composition effects in a variety of crustal magma types. Earth Planet Sci Lett 64:295–304

Watson EB, Harrison TM (2005) Zircon thermometer reveals minimum melting conditions on earliest Earth. Science 308:841–844

Watson EB, Lupulescu A (1993) Aqueous fluid connectivity and chemical transport in clinopyroxene-rich rocks. Earth Planet Sci Lett 117:279–294

Watson EB, Cherniak DJ, Hanchar JM, Harrison TM, Wark DA (1997) The incorporation of Pb into zircon. Chem Geol 141:19–31

Wiedenbeck M, Allé P, Corfu F, Griffin WL, Meier M, Oberli F, von Quadt A, Roddick JC, Spiegel W (1995) Three natural zircon standards for U-Th-Pb, Lu-Hf, trace element and REE analyses. Geostand Newslett 19:1–23

Wilde SA, Valley JW, Peck WH, Graham CM (2001) Evidence from detrital zircons for the existence of continental crust and oceans on the Earth 4.4 Ga ago. Nature 409:175–178

Wilson CJN, Hildreth W (1997) The Bishop Tuff: new insights from eruptive stratigraphy. J Geol 105:407–439

Wong L, Davis DW, Krogh TE, Robert F (1991) U-Pb zircon and rutile geochronology of Archean greenstone formation and gold mineralization in the Val d'Or region, Quebec. Earth Planet Sci Lett 104:325–336

Wyllie PJ (1983) Experimental and thermal constraints on the deep-seated parentage of some granitoid magmas in subduction zones. In: Atherton MP, Gribble CD (eds) Migmatites, melting and metasomatism. Shiva, Cheshire, pp 37–51

Zack T, Kronz A, Foley SF, Rivers T (2002) Trace element abundances in rutiles from eclogites and associated garnet mica schists. Chem Geol 184:97–122

Zack T, Moraes R, Kronz A (2004) Temperature dependence of Zr in rutile: empirical calibration of a rutile thermometer. Contrib Mineral Petrol 148:471–488